F3

Faculty of Electrical Engineering
Department of Electromagnetic Field

Master's Thesis

Modeling of Probes and Correction Methods for Microwave Measurements at Probe Stations

Bc. Jan Šmolcnop
Electronics and Communications - Radio Communications and Systems

May 2024
Supervisor: Ing. Viktor Adler, Ph.D.

MASTER'S THESIS ASSIGNMENT

I. Personal and study details

Student's name: **Šmolcnop Jan** Personal ID number: **492066**

Faculty / Institute: **Faculty of Electrical Engineering**

Department / Institute: **Department of Electromagnetic Field**

Study program: **Electronics and Communications**

Specialisation: **Radio Communications and Systems**

II. Master's thesis details

Master's thesis title in English:

Modeling of Probes and Correction Methods for Microwave Measurements at Probe Stations

Master's thesis title in Czech:

Modelování sond a korekčních metod pro mikrovlnná měření na probe station

Guidelines:

Design and manufacture a fixture to mount and place the Form Factor ACP65-AW-GSG-250 and ACP110-AW-GSG-100 air coplanar probe under the microscope. Using a microscope, measure the dimensions of the probes with particular attention to the geometry of the tips and model the probes in the CST Studio Suite software. Perform a 3D EM simulation of the probes confirming the integrity and correctness of the created models. Furthermore, implement correction methods based on open, short and thru circuit measurements and compare the methods with each other. Apply the correction to the simulated models of the capacitor and inductor fabricated on alumina.

Bibliography / sources:

[1] Rumiantsev, A., Doerner, R.: RF Probe Technology: History and Selected Topics, in IEEE Microwave Magazine, vol. 14, no. 7, pp. 46-58, Nov.-Dec. 2013
[2] Lourandakis, E.: On-Wafer Microwave Measurements and De-embedding, Artech House, 2016
[3] Rumiantsev, A.: On-Wafer Calibration Techniques Enabling Accurate Characterization of High-Performance Silicon Devices at the mm-Wave Range and Beyond, dissertation thesis, River Publishers, 2019
[4] Schmückle, F. J., Doerner, R., Phung, G. N., Heinrich, W., Williams, D. and Arz, U.: Radiation, multimode propagation, and substrate modes in W-band CPW calibrations, 2011 41st European Microwave Conference, Manchester, UK, 2011, pp. 297-300
[5] Aguilera, J., Berenguer, R.: Design and Test of Integrated Inductors for RF Applications, Kluwer Academic Publishers, 2004

Name and workplace of master's thesis supervisor:

Ing. Viktor Adler, Ph.D. Department of Electromagnetic Field FEE

Name and workplace of second master's thesis supervisor or consultant:

Date of master's thesis assignment: **19.02.2024** Deadline for master's thesis submission: _____

Assignment valid until: **15.02.2026**

Ing. Viktor Adler, Ph.D. Supervisor's signature	Head of department's signature	prof. Mgr. Petr Páta, Ph.D. Dean's signature

III. Assignment receipt

The student acknowledges that the master's thesis is an individual work. The student must produce his thesis without the assistance of others, with the exception of provided consultations. Within the master's thesis, the author must state the names of consultants and include a list of references.

Date of assignment receipt	Student's signature

Acknowledgement / Declaration

I would like to express my gratitude to my supervisor, Ing. Viktor Adler, Ph.D., for his guidance and support throughout this Master's thesis. His patience and insightful advice have been invaluable in shaping this research. I am deeply appreciative of the time he dedicated to me, which greatly contributed to successful completion of the thesis. Additionally, I extend my thanks to my family for their support and encouragement during this academic journey. Their backing has been a cornerstone of my success.

I declare that I have written submitted thesis by myself and that I have listed all information sources in accordance with Methodical Guideline on Compliance with Ethical Principles.

In Prague: 24. May 2024

.....

Abstrakt / Abstract

Práce se zaměřuje na modelování a simulaci koplanárních vlnovodných sond a metody de-embeddingu používaných pro měření planárních struktur vyrobených na korundu. 3D modely sond mohou být užitečné pro simulace při návrhu planárních struktur nebo charakterizaci vysokofrekvenčních zařízení. De-embedding je matematický proces získání S-parametrů zařízení z měřené struktury ovlivněné parazitními impedancemi kontaktních plošek a spojovacích vedení. Cílem je implementovat tyto metody a otestovat jejich funkčnost v EM simulaci na planárním kondenzátoru a induktoru vyrobených tenkovrstvou technologií na korundu v kombinaci s modelem koplanární vlnovodné sondy.

Klíčová slova: Vzduchové koplanární sondy, 3D model mikrovlnné sondy, OPEN-SHORT de-embedding, THRU de-embedding, Elektromagnetická simulace planárních struktur

Překlad titulu: Modelování sond a korekční metody pro mikrovlnná měření na probe station

The thesis focuses on modeling and simulation of coplanar waveguide probes and de-embedding methods used for measurements of planar structures fabricated on alumina. 3D models of probes can be useful for simulations during the design process of planar structures or characterisation of high frequency devices. The de-embedding is a mathematical process of extracting S-parameters of a device from measured structure influenced by parasitic impedances of contact pads and connecting lines. The goal is to implement these methods and test their performance in EM simulation on planar capacitor and inductor fabricated by thin-film technology on alumina substrate in combination with the model of the coplanar waveguide probe.

Keywords: Air Coplanar Probes (ACP), Microwave Probe 3D Model, OPEN-SHORT De-Embedding, THRU De-Embedding, EM Simulation of Planar Structures

Contents /

1 Introduction 1

2 On-Wafer measurement 2

2.1 Probe Station 2

2.2 Microwave Probes 3

2.2.1 Basic Design of High Frequency Measuring Probes 4

2.2.2 Probe Characteristics 5

2.2.3 Picoprobe 6

2.2.4 Air Coplanar Probe (ACP) . 6

2.2.5 |Z|-Probe 7

2.2.6 Infinity Probe 8

2.3 Calibration Substrates 8

2.3.1 Calibration Standards 8

3 3D Model Development for Simulations 10

3.1 Fixture 10

3.2 3D Model 11

3.2.1 Coaxial Adapter 12

3.2.2 Microcoaxial Cable 14

3.2.3 Air Coplanar Tip 14

4 Probe Simulation 16

4.1 Coplanar Waveguide 17

4.2 Simulation Results 17

5 Calibration and Correction of Simulated Data 19

5.1 Models of Calibration standards 19

5.1.1 Unknown Thru 20

5.1.2 Open 21

5.1.3 Short 21

5.1.4 Match 22

5.2 Calibration Validation 23

6 De-Embedding 25

6.1 OPEN-SHORT De-Embedding 26

6.2 THRU De-Embedding 28

7 Design of Simulated DUTs 30

7.1 Inductor 30

7.1.1 RAW 30

7.1.2 OPEN 31

7.1.3 SHORT 31

7.1.4 THRU 32

7.2 Capacitor 32

7.3 Reference Devices 32

7.3.1 Reference Inductor 33

7.3.2 Reference Capacitor 33

8 Results of Implemented De-Embedding Methods 35

8.1 UOSM Calibration 35

8.2 Inductor 35

8.3 Capacitor 36

8.4 Inductor and Capacitor Measurement Conclusion 38

8.5 CPW Line 39

9 Conclusion 43

References 44

A MATLAB Script OPEN-SHORT De-Embedding 47

B MATLAB Script THRU De-Embedding 48

Chapter 1
Introduction

In the rapidly advancing field of high-frequency electronics, the characterisation of electronic components is crucial for the development of efficient and reliable devices. The usage of microwave probes plays an important role in the precise measurement and characterisation of both passive and active devices such as inductors, capacitors, transmission lines or transistors. Probes provide testing of the electronic components directly on their substrates, enabling the evaluation of their performance without the need for packaging and assembly. This is particularly beneficial for the radio frequency integrated circuit engineers that rely on accurate device models and measurements for the design of complex circuits [1].

At high frequencies, the measurement and characterisation of planar structures poses significant challenges due to the parasitic effects of pads and leads. These parasitic characteristics, including unwanted capacitance, inductance, and resistance, can distort the true electrical performance of the device under test. These effects become particularly notable at microwave frequencies, where even minor parasitic elements can significantly affect measurement accuracy. To mitigate these issues, de-embedding structures are employed. De-embedding is a technique that involves the use of specially designed de-embedding structures and mathematical procedures to separate and remove the parasitic contributions of the measurement setup from the DUT. By accurately characterising and accounting for the parasitic parameters, de-embedding ensures that the measurements reflect the properties of the DUT, thereby enhancing the reliability and precision of the characterisation process.

Simulation tools can be used to model the entire measurement setup, including the microwave probes, connection pads, and the DUT. By accurately replicating the measurement environment, engineers can predict the performance of their designs. This capability not only accelerates the design process but also reduces development costs by minimising the number of required physical prototypes.

De-embedding is a well-established technique in the field of integrated circuits. It has proven well designed for ensuring the precise characterisation of IC components. However, the application of de-embedding techniques has been relatively limited when it comes to planar devices fabricated by thin-film technology. The goal of this thesis is to discover the possibilities of using these methods on passive planar devices fabricated on alumina substrate.

Chapter 2
On-Wafer measurement

On-wafer measurement is a technique used in the design and manufacture of high-frequency integrated and planar circuits. This method enables the direct testing of circuit parameters and functionality on the substrate, eliminating the need to cut the entire chip from the wafer, mount it in a housing, and connect it to a printed circuit board. This streamlined process significantly reduces test and design time, thereby lowering the overall cost of the development and manufacturing process.

Additionally, on-wafer measurement is invaluable for inspecting circuits directly on the production line, a process that can be fully automated. This capability allows for real-time quality control and early detection of defects, which enhances the efficiency and reliability of production. The ability to test and validate circuits at this early stage ensures that only fully functional chips proceed to further stages of production, thereby minimising waste. Incorporating on-wafer measurement techniques into the design and manufacturing workflow not only accelerates the development cycle but also provides a cost-effective solution for maintaining high standards of quality and performance in high-frequency circuit production.

It is not just a matter of verifying entire circuits, but the first step in designing a functional device are accurate models of the high-frequency components used. It is therefore important to have the technology to characterise these components accurately and efficiently.

2.1 Probe Station

Wafers with radius typically from 100 mm to 450 mm and thickness of 0.5 mm must be handled with great care. More than 400 chips can be printed on a wafer with dimensions in micrometres. Therefore, a special equipment is required for gentle and precise manipulation. Probe station is a precision mechanical apparatus for providing repeatable and controllable handling of wafers, probes and substrates involved in the on-wafer measurement procedure. It integrates all the functionality needed for positioning, inspecting and probing silicon-integrated devices. Silicon wafers (or chips themselves) are fixed on a chuck. This is a pad that uses vacuum conditions or mechanical clamping to hold the test object in place, which is crucial when it comes to accurate and repeatable touchdown of a probe. Probe station also provides mounting points for the probes which are mechanically controlled by micrometre manipulators in all three axes and typically observed under the microscope [1].

Semi-automatic or fully automatic probe stations are much more complex. They use software-controlled steppers and in combination with a digital microscope the software can position the probes for the best repeatable contact. Another functionality is wafer map creation, a process where the software is able to map the individual circuits or even sub-circuits of the wafer based on the image from the digital microscope. Furthermore, it can also identify individual IC blocks. In more advanced cases, probe station uses a

metallic cage around the chuck providing electromagnetic shielding against interference. This can also be used to control the temperature for more precise measurements.

In summary, manual probe stations are typically used for entry-level characterisation in academic or industrial laboratories. Semi-automatic or automatic stations find their utilisation in characterisation of mass production. Here the entire process of measurement can be automated from calibration to measurement cycles, increasing efficiency and improving the contact repeatability.

2.2 Microwave Probes

For on-wafer measurements, a microwave probe is essential due to its ability to accurately measure high-frequency signals directly from the DUT. Various types of probes are available, tailored to specific applications. These range from DC probes, which provide power to the DUT, to RF probes, which are specifically designed for measuring high-frequency signals with precision [2]. The focus of this thesis is on RF probes, which are critical for ensuring a well-matched transition from coaxial cables to coplanar lines. This well-matched transition is necessary to minimise reflection and signal degradation, which are particularly problematic at high frequencies.

Microwave probes are useful not only for on-wafer measurements but also for ordinary planar measurements (on microstrip or coplanar waveguide), making them versatile tools in the characterisation of high-frequency devices. Their ability to provide accurate and repeatable measurements of high-frequency signals is essential for the characterisation and validation of planar structures and other high-frequency devices. Without microwave probes, achieving precise measurements would be challenging, thus impeding the development and testing of such devices. Figure 2.1 illustrates examples of microwave probes from FormFactor, Inc., highlighting their role in facilitating precise on-wafer and planar measurements.

Figure 2.1. Example of different types of microwave probes. From the left, two ACP probes and a T-wave probe (waveguide excitement). Source: [3].

High-frequency measurements on substrate cannot be made in the same way as low-frequency measurements using thin sharp probes (like needles). The main reasons are the self inductance, mutual inductance and capacitance between the tips and between the tips and the substrate itself. There would be very strong undesirable crosstalk between the probes, they would be very poorly matched and the measurement of the S-parameters would be non-repeatable [4]. From these observations, the basic rules for substrate measurements follow [2]:

- The 50-Ω planar transmission line of the probe should be brought in contact with DUT pads directly, without contact wires.
- Tilting of the probe is required to contact the DUT signal and ground pads simultaneously. This procedure is called “probe planarization.”

- The contact repeatability of the probe is much better than that of the coaxial connector. This finding has facilitated the development of probe tips and on-wafer standards and dedicated calibration methods.
- The high contact repeatability allowed accurate calibration of the probe and shifting of the measurement reference plane to its tips.
- It was demonstrated that, due to their small geometrical sizes, an equivalent model of planar standards can be assumed to be purely lumped. Moreover, model parameters can easily be predicted from geometrical dimensions of the standard.

Coplanar probes are commonly used, i.e. the probe tip is shaped in such a way that the probe can be connected to the coplanar line. An example of such a geometry is shown in Figure 2.2. Pitch of the probe is a dimension, which is specified by the manufacturer. It is the distance between the centres of the probe's signal and ground tip.

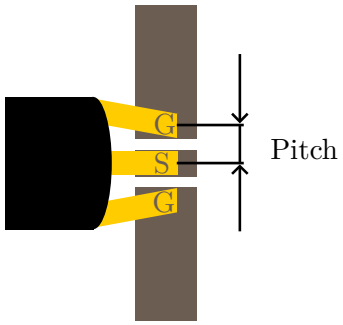

Figure 2.2. Example of a simple geometry of a GSG coplanar probe connected to a coplanar line.

Another terms used with regard to probes are skate and overtravel. To ensure proper connection it is necessary to press the probe to the contact pads, in a predefined manner, after touchdown. Skate and overtravel are given by the manufacturer for every probe. In the Figure 2.3 both parameters are illustrated. Overtravel is the distance in z-coordinate of how much the probe's body moves. As the tip is pressed into the contact pad, the microcoaxial cable bends and allows the tip to move forward. This is called skate.

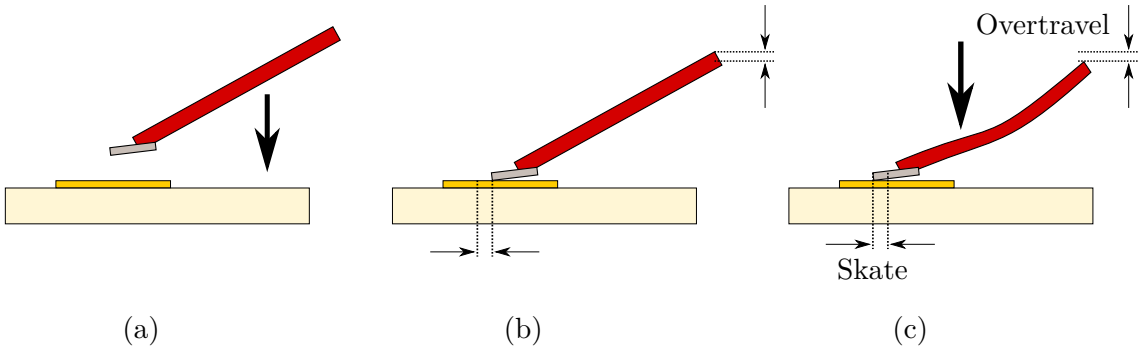

Figure 2.3. Stages of probe connecting to a pad. (a) probe descending, (b) probe touches pad, (c) probe pressed for proper contact.

2.2.1 Basic Design of High Frequency Measuring Probes

The purpose of a microwave probe is to transform an electromagnetic wave guided on a coaxial line (or waveguide) into a two-dimensional medium, a planar line (coplanar line,

or microstrip). A conventional microwave probe structure is illustrated in Figure 2.4. During the transition, it is important that the line always has the same characteristic impedance Z_0 (typically 50 Ω). The probe inputs are generally standardised coaxial or waveguide connectors, and the transition to a planar structure introduces discontinuities into the system where higher modes of electromagnetic waves can originate. These other modes are undesirable, and the design goal is to prevent them from occurring, or at least to suppress them as much as possible. Absorbing materials are used to prevent the electromagnetic field propagating from the probe tip from interacting with the measured DUT.

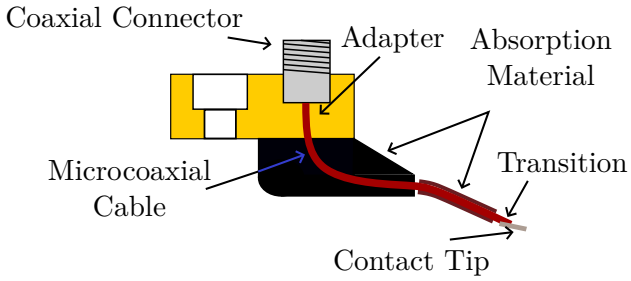

Figure 2.4. Typical microwave probe design model.

Nowadays there are many different microwave probe concepts. For example, it is possible to avoid the micro-coaxial cable and switch from a coaxial (or waveguide) connector directly to a planar line. This approach is used by |Z|-Probe probes (see section 2.2.5). This can reduce the insertion loss that the micro-coaxial cable causes but sacrifices the mechanical properties of the probe.

Also, the tips can have different geometries of design and attachment (several examples are shown in Figure 2.5). The differences arise from the trade-off between mechanical and electrical properties, and from the material of the tip and contact plates of the measured DUT.

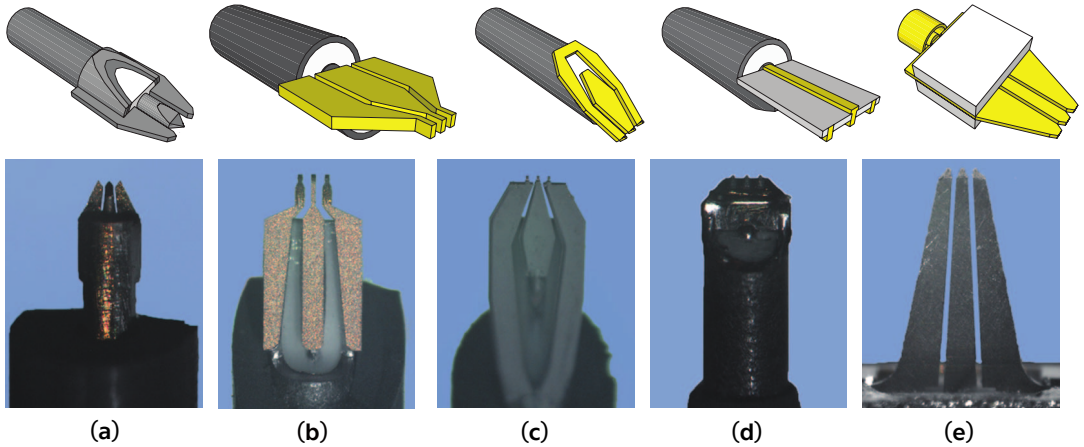

Figure 2.5. Example of different GSG tip designs: (a) Picoprobe (top view, 100 μm pitch), (b) ACP (125 μm pitch), (c) Allstron (100 μm pitch), (d) Infinity Probe (125 μm pitch), (e) |Z|-Probe (125 μm pitch). Source: [2].

2.2.2 Probe Characteristics

With RF probes, the specified and usable performance range is based on combination of multiple probe attributes. The dominant characteristic that limits the frequency range

is the coaxial connector used. However, other attributes impact the probe bandwidth or upper frequency [3].

As already mentioned, coaxial connector is the major decisive factor. In the Table 2.1 are mentioned some of the most used connectors and their upper frequency limit for best case scenario. Of course in the design process of microwave probe the connector is chosen with regard to the whole package, that consists of microcoaxial cable dimensions, tip geometry, etc.

Table 2.1. Table of coaxial connectors and their upper frequency limitations [3].

Connector Type	Frequency limit
2.92 mm/K connector	40 GHz
2.4 mm	50 GHz
1.85 mm	67 GHz
1 mm	110 GHz (extended 130 GHz)
0.8 mm	145 GHz

Tip configuration also influences the frequency performance of the whole probe. For single line probes, two styles are possible. Balanced GSG (Ground Signal Ground) contacts offers best performance, but contact pads take up more space on the measured device. On the other hand, GS or SG configurations can reduce usable frequency range. For dual line probes the limiting parameter is crosstalk between the signal lines. Once again balanced GSGSG combination offers the best performance. However, unbalanced GSSG configuration can also deteriorate the frequency range in most cases. Tip configuration is closely related with the probe's pitch. Wide pitches increase the ground path inductance, thus again limit the available bandwidth. For instance, for frequency ranges up to 40 GHz pitches less than 250 μm are recommended. With higher frequency, smaller pitches may be required to maintain suitable electrical characteristics. As the pitch dimension becomes a significant percentage of the wavelength of the measured frequency, occurrence of higher modes is possible. Typical tip pitch for ACPs ranges from 50 μm to 250 μm.

Other parameters to look for are for example tip material, which depends on the material of contact pads of the measured device, maximal DC current, maximal RF power, insertion loss, return loss, operating temperature or number of repeatable connections.

2.2.3 Picoprobe

One of the first microwave probes, introduced in 1988 by GGB Industries. Compared to the earlier probes with ceramic tips, which were very fragile and easily broken, this type had a great advantage in terms of mechanical properties. The probe tip is formed by extending the coaxial conductors and bending the ground straps to make them flexible. The process of connection to the DUT touch pads is shown in Figure 2.7. By pressing the probe to the pads, the ground straps are bend slightly allowing the centre conductor to also connect [2].

2.2.4 Air Coplanar Probe (ACP)

This probe was first introduced by Cascade in 1994 [6]. The probe concept is very similar to the one in Figure 2.4, except the tip is formed by an air coplanar line (Figure 2.5 (b)). It is made of either tungsten (W) or beryllium copper (BeCu) depending on the material of the contact plates of the DUT. Tungsten is specified for aluminium pads

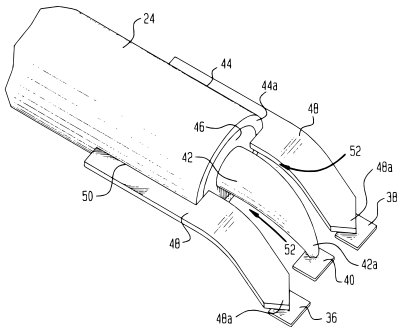

Figure 2.6. Tip of a high frequency probe Picoprobe. Source: [5].

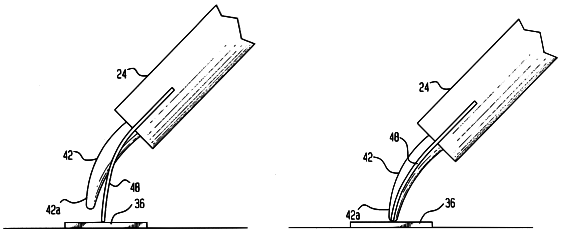

Figure 2.7. Connection of the probe to DUT's contact pads. On the left before being connected and on the right after. Source: [5].

and beryllium copper is specified for gold pads. To increase conductivity, beryllium copper or tungsten is plated with gold. The design of the tip and choice of material ensures good mechanical properties. As a result, accurate repeatable measurements can be obtained even on tilted surfaces. Such that are rotated in the perpendicular direction to the centre conductor axis, so that the ground conductors are at different heights [6].

To this day, ACPs are still the preferred type of high frequency probes when measuring on gold wiring due to the soft touch that does little to wear the touch pads.

2.2.5 |Z|-Probe

In 2001, Rosenberger and SUSS MicroTec introduced the first |Z|-Probe with a frequency range up to 40 GHz. The main ideas were the following [2]:

- The probe was designed without the microcoaxial cable. It was realised by direct transition from the coaxial connector to air coplanar waveguide inside the probe.
- This transition was made within the probe body, which allows a precise optimisation of the transition point, minimising possible discontinuities.
- The coplanar contacts were fabricated using an ultraviolet lithography and electroplating process (UV-LIGA) that is very similar to the one used for fabricating MEMS components. Extremely high accuracy and repeatability of the process provided very accurate shape of the CPW line and a constant air gap.

As a result, it was possible to extend the coplanar tip without compromise in increasing the return loss due to a very good match. The probe also had very good mechanical properties, e.g. long lifetime (more than one million connections), a maximum „overtravel“ of up to 200 μm and the ability to connect to touch pad devices at different heights by up to 50 μm. The probe tip is shown in the Figure 2.5 (e).

2.2.6 Infinity Probe

In response to the shrinking contact area of the DUTs, in 2002 Cascade Mircotech introduced a new probe based on thin film technology. A microstrip line on a flexible substrate transmits signal from the coaxial line to the measured device. The contact area of the probe tip was approximately μm $\times$ 12 μm, which allowed the probe to be connected to very small areas. The advantage was a repeatable connection with high accuracy and very low crosstalk. These features made the probe the standard for measuring high Q passive circuits and small active MOS devices [2].

2.3 Calibration Substrates

To calibrate measurement setup directly at the probe tip, there are available on-wafer calibration kits. The commercial version of these kits is known as Impedance Standard Substrate (ISS). These ISSs are available in a number of configurations depending on the used probe configuration (G-SG, G-S, S-G-S, ...) and the desired form of calibration (UOSM, LRM, ...). They are usually implemented on an alumina substrate with low loss factor and high dielectric constant. Metallisations are manufactured from gold for low contact resistance and oxidation [7]. Their electrical behaviour can be derived from their physical geometry, which enables the determination of systematic errors within the measurement setup. Manufacturers determine their parameters, which are then used in the calibration process [1].

For each type of RF probes a calibration substrate is available depending on the tip geometry, pitch, working frequency or tip material. In the Figure 2.8 is an example of calibration substrate 104-783 fabricated on alumina from vendor FormFactor, Inc. for probes with pitch $75 - 150$ μm, frequencies up to 145 GHz.

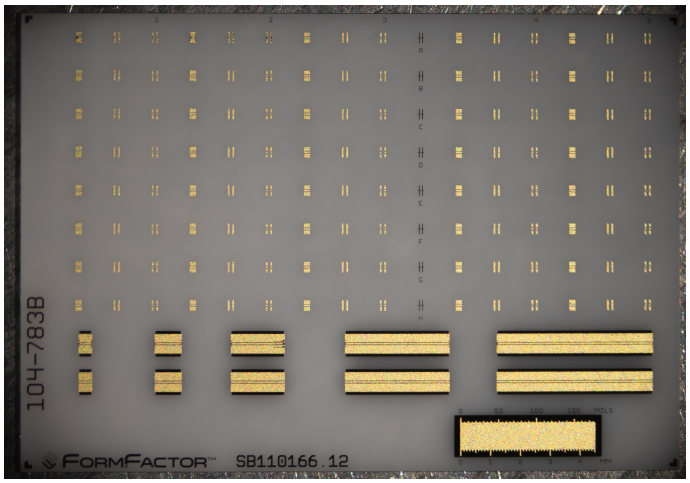

Figure 2.8. Photo of calibration substrate 104-783 of manufacturer FormFactor, Inc. for the probe ACP110-AW-GSG-100. Photo Adler Viktor.

2.3.1 Calibration Standards

The basics of calibration standards for on-wafer measurement are equivalent to well-known coaxial standards. The fundamental being the open standard. It can be realised as a very short part of a coplanar line, but its measurement is often performed by lifting the probes off the substrate. Dominant characteristic of the open is its parasitic

capacitance formed between the signal strip (or tip) and the grounds. The capacitive behaviour can be observed on the Smith chart, starting at the infinite impedance and then moving clockwise with increasing frequency. The standard is then characterised by a value of capacitance. For calibration where probes are raised in the air then the capacitance is negative. This is caused by the different wave propagation speeds, with waves travelling faster in the air than on the alumina substrate [1].

Similarly short is simply a metal strip connecting the signal and ground probe tips. It is characterised by its parasitic inductance L, which is caused by the metal strip between signal pin and the two grounds.

Standard match is ideally 50 Ω load connected to the ground without any frequency dependence so in the Smith chart its reflection would be displayed as a point in the middle, representing a perfectly matched device. However, the actual non-ideal metallisation introduces a parasitic inductance and resistance between the contacts. In coplanar technology the 50 Ω load is formed out of two 100 Ω resistors connected in parallel, both between the signal and a ground strip [1].

Last measurement standard is thru, that connects the signal pins and ground pins of two GSG probes. Generally thru is implemented as a coplanar waveguide transmission line of certain length, with impedance of 50 Ω and matches the pitch dimensions of the coplanar probe.

Chapter 3
3D Model Development for Simulations

Nowadays, manufacturers of high-frequency equipment are highly protective of their trade secrets, making it challenging to obtain detailed characteristics of microwave probes. This lack of detailed information brings significant difficulties, especially in calibration and accurate measurements. Accurate measurement and interpretation of measured data require a comprehensive understanding of the measuring equipment. Without this, it is impossible to differentiate between errors originating from the device under test (DUT) and those from the measurement setup. To verify measurement accuracy, it is often useful to run simulations beforehand to establish expected results. However, manufacturers typically do not provide 3D models for their products, necessitating the creation of these models independently. This additional step is crucial to ensure that the simulations accurately reflect the behaviour of the physical probes, thereby enabling precise calibration and reliable measurements.

The actual modeling was preceded by the design and manufacture of a specialised fixture, which allowed for the precise fitting of the probe and the accurate measurement of its dimensions under a microscope. This fixture was essential for capturing the critical geometries required for accurate simulation and modeling. The most crucial component to measure accurately was the coplanar tip, as its exact dimensions are not provided by the manufacturer. By using this fixture, detailed and precise measurements of the coplanar tip were obtained, ensuring that the subsequent modeling in the simulation environment would closely replicate the actual physical characteristics of the probe. This step was crucial for achieving high precision in the simulation results and for ensuring that the calibration and measurement processes would be as accurate as possible.

3.1 Fixture

As mentioned above, it was necessary to create a fixture in which the probe could be securely placed. The primary objective was to design the fixture for practical use, while also protecting the probe tip from potential damage. The tip of the probe is quite fragile, and even a careless touch could break or bend it, making the probe unusable. The fixture not only facilitated the accurate measurement of the probe's dimensions but also ensured that the probe could be handled safely and efficiently.

In terms of probe handling, the mount had to be designed to allow the probe to be viewed under the microscope from different angles and sides. A sphere composed of triangles was found to be the most suitable shape for this purpose. This shape was generated in MathWorks MATLAB software using the function *icosphere*[1] (see Figure 3.1). The generated sphere was then exported as a *.stl* file to CST Studio Suite software for further editing. In the sphere, several adjoining triangles were removed at appropriate locations to create windows through which the probe tip could be accurately

[1] Function available at: `https://www.mathworks.com/matlabcentral/fileexchange/50105-icosphere`

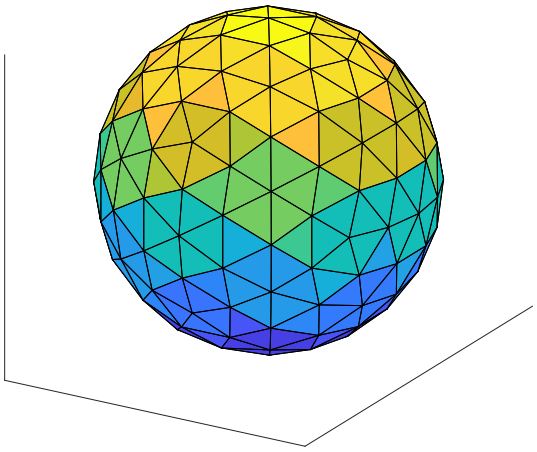

Figure 3.1. A sphere generated in MathWorks MATLAB software and used to create a probe fixture.

measured. This design ensured that the probe tip could be carefully examined and measured from multiple perspectives without risking damaging the probe.

The next task was to design a system of fixing the probe in the holder. For this purpose, the protective packaging in which the manufacturers normally supply the probes served as an inspiration. The probe is placed on the base, anchored with two pins through the outermost mounting holes in the probe and secured with a screw through the middle hole. The probe attachment works very similarly. Holes were prepared inside the model into which the nuts were inserted during the printing process so that they remain firmly attached inside the printed fixture. The outermost anchor pins have a short thread, so they screw into the inserted nuts. The middle hole secures the probe with a wing screw. This whole part is printed separately and attached to the sphere with two small screws.

Subsequently, a system for securely fixing the probe within the holder. A protective packaging provided by manufacturers for the probes served as an inspiration for this design. In this packaging, the probe is placed on a base, anchored with two pins through the outer mounting holes, and secured with a screw through the middle hole.

For a practical use of the fixture, the sphere was divided into two parts by a cut approximately in the middle. Small holes were prepared at four points of contact between the two halves, for the placement of magnets to securely hold the sections together. This design enables easy opening and closing of the fixture, ensuring convenient manipulation of the probe while maintaining the integrity and alignment of the structure. The final model is pictured in Figure 3.2.

3.2 3D Model

Two types of coplanar probes were modelled. The first probe, ACP65-AW-GSG-250 (as illustrated in Figure 3.3), is designed to operate up to 65 GHz. It is equipped with a 1.85 mm connector and has a pitch of 250 μm, making it suitable for precise high-frequency measurements. The second probe, ACP110-AW-GSG-100, is engineered to function up to 110 GHz. It features a 1 mm connector and a finer pitch of 100 μm,

Figure 3.2. Photo of the 3D printed probe fixture. Photo author.

allowing for even higher frequency applications. Both probes are fitted with tungsten tips, chosen for their durability and excellent conductive properties.

The models of these probes include several components: a coaxial adapter, a microcoaxial cable, and an air coplanar probe tip. The coaxial adapter is a standard in microwave measurement setup and ensures a secure and reliable connection to the measurement equipment. The microcoaxial cable provides flexibility and minimises signal degradation, while the air coplanar probe tip enables accurate contact with the DUT. Each of these components is crucial for achieving precise and reliable high-frequency measurements. The design and specifications of these parts will be elaborated upon in the following sections. As it has already been mentioned, there are no official detailed datasheets describing the design, so the geometrical properties of these components must have been reverse engineered.

3.2.1 Coaxial Adapter

Due to the differing dimensions of the connector and the micro-coaxial cable, it was necessary to ensure proper impedance matching between the two lines. Given that the internal structure of the probe is unknown, the transition was designed to achieve a S_{11} across the entire frequency band that is lower to that of the probe as a whole. The design of these transitions is illustrated in Figure 3.4. The transitions employ a simple step design, where the lower capacitance between the narrower centre conductor and the wider outer conductor is balanced by the increased capacitance resulting from the wider centre conductor and the narrower outer conductor. The optimisation process for the transition focused on determining the optimal dimension of the parameter d, which represents the length of the overlap between the narrower centre conductor and the wider outer conductor. This careful optimisation ensures minimal reflection and maximises the performance of the transition across the specified frequency range

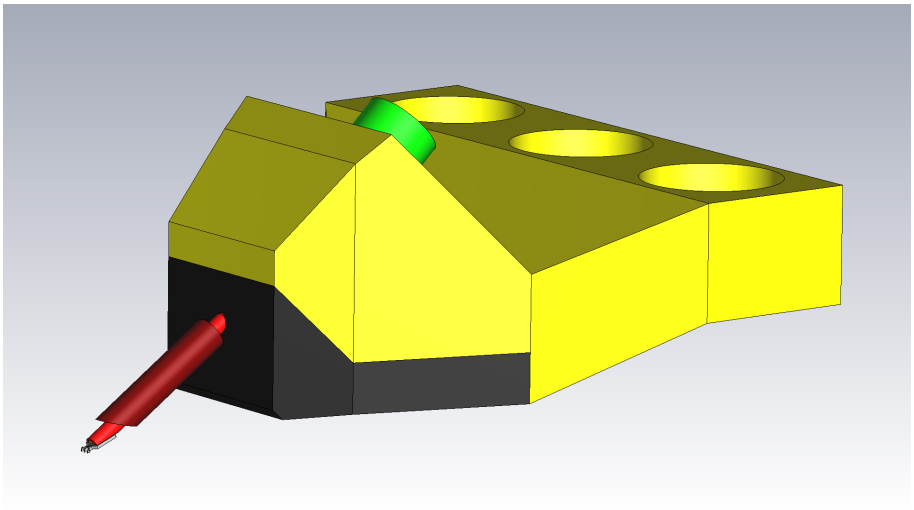

Figure 3.3. 3D probe model ACP65-AW-GSG-250 in CST Studio Suite, the second model ACP110-AW-GSG-100 is almost identical, except for the connector and coplanar tip.

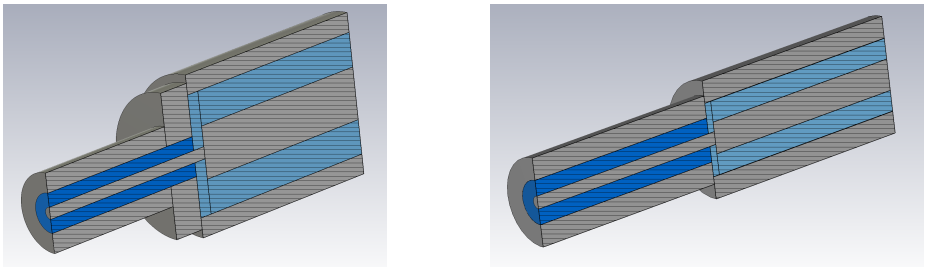

Figure 3.4. Cross section of the coaxial transitions between the microcoaxial cable connecting the probe tip and the connector. (a) 1.85 mm connector, (b) 1 mm connector. The light blue part is the dielectric of the connector, i.e. air.

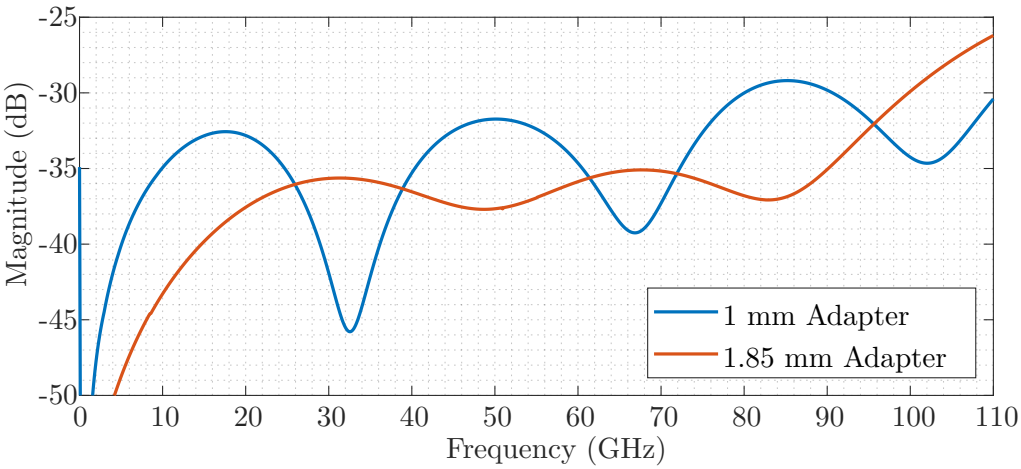

Figure 3.5. Simulation results of magnitude S_{11} of coaxial transitions in CST Studio Suite without considering losses.

The resulting S_{11} of both transitions is shown in Figure 3.5, where the requirement was to obtain a reflection better than -20 dB over the whole frequency band.

3.2.2 Microcoaxial Cable

When modeling this part, determining the precise dimensions of the conductors proved challenging. Firstly, the cable is not cut exactly in the middle when viewed from the front, making it impossible to measure the radius directly. Secondly, the inner conductor is not visible at all, further complicating accurate dimension measurement (see Figure 3.6). These issues necessitated the use of indirect methods and estimations to derive the necessary parameters for accurate modeling and optimization of the transition between the connector and the microcoaxial cable.

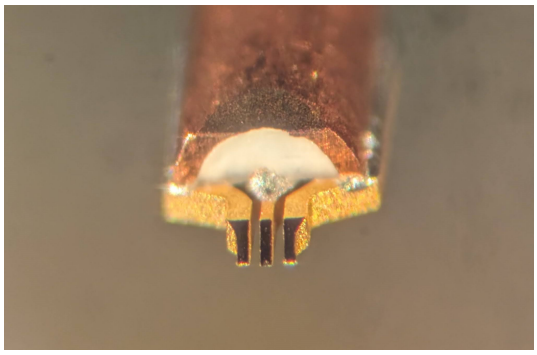

Figure 3.6. Front view of the ACP110-AW-GSG-100 probe tip and microcoaxial cable. Photo author.

The radius of the outer conductor was calculated based on the assumption, that its shape is a circle and a part of its circular cross-section can be seen. A circle can be uniquely defined by three separate points that lie on it. This geometric principle can be used in determining the circle's radius and centre from three measured points. By using the coordinates of these three points, the equation of the circle can be derived, which provides the radius and the centre of the circle. This method was employed to calculate the radius of the outer conductor in the described modeling process. By measuring the coordinates of three points that lie on the inner part of the outer conductor, it was possible to determine both the radius and the coordinates of the centre of the circle. The calculated radius for both types of probes is 0.6 mm.

Subsequently, the radius of the inner conductor was then determined, assuming a cable impedance of 50 Ω and a Teflon dielectric with $\epsilon_r = 2.1$. Its diameter was found to be 0.091 mm. The model of the whole line is shown in Figure 3.7.

3.2.3 Air Coplanar Tip

Modeling the probe tips happened to be the most challenging part of the models. Especially because of its miniature dimensions that were very hard to accurately measure and replicate in the CST Studio Suite environment. Moreover, from an electromagnetic perspective, achieving precise measurements and subsequent modeling of the transition from coaxial to coplanar conduction was crucial. This transition was meticulously examined under a microscope. The probe tip comprises one signal line and two ground lines, connected to a cut coaxial cable at an angle of 12°. Both types of probes feature conductors with a width of 50 μm at the tip, yet their geometries and the distances between the signal and ground tips differ due to variations in pitch. Interestingly, the coaxial cable is not completely cut; instead, it is rounded at the point where the probe tip ends. Additionally, in the ACP110-AW-GSG-100 model, the outer wire is cut from the top, likely to minimize the influence of the field coupled from the coaxial cable directly to the coplanar line.

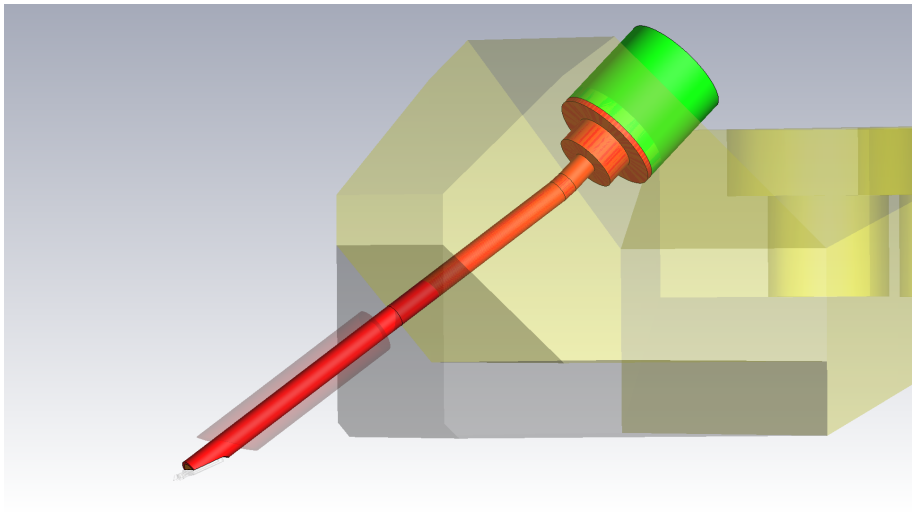

Figure 3.7. View of the internal structure of the connector, transition and microcoaxial cable of the ACP65-AW-GSG-250 probe in CST Studio Suite, the second model ACP110-AW-GSG-100 is almost identical except for the size of the connector and coplanar tip.

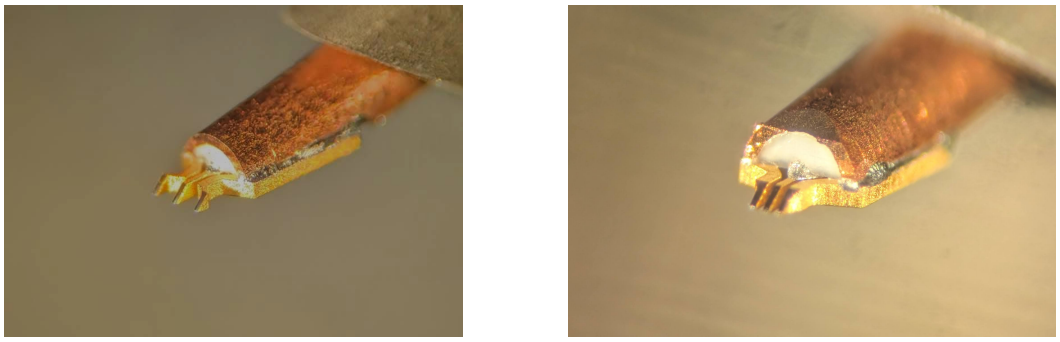

(a) (b)

Figure 3.8. View of the tips of both probes. (a) ACP110-AW-GSG-100, (b) ACP65-AW-GSG-250. Photo author.

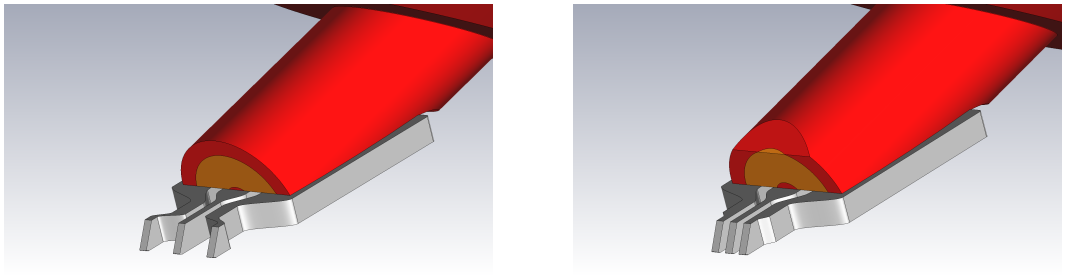

(a) (b)

Figure 3.9. Tip model of both probes. (a) ACP110-AW-GSG-100, (b) ACP65-AW-GSG-250.

A view of the coplanar tips is shown in Figure 3.8 and their models are shown in Figure 3.9.

Chapter 4
Probe Simulation

To verify the functionality of both models, simulations of two probes connected to a coplanar line were performed. The lines have the same parameters as the manufacturer's calibration set, i.e., the width of the centre conductor, the width of the gap between the centre and ground conductors, and the relative permittivity of the substrate. The only difference is that in the simulations the substrate's height is doubled and the boundary condition „open“ is used. This is because in real measurements a substrate of different materials (metal, ceramic, or absorbing material) is used under the calibration set (or the circuit to be measured). According to [8], metal has the worst properties for measurements above 60 GHz and is not suitable for calibration. A pad of lossy material has better properties but affects the characteristic impedance of the line and increases the attenuation constant non-linearly. In addition, simulating a line with an absorption pad would be very computationally challenging, as generally lossy structures are difficult to simulate. The ceramic material should limit the occurrence of higher modes without adversely affecting the properties of the coplanar line. Therefore, doubling the height of the substrate and the boundary condition will ensure that most of the energy transferred by the field will remain within the substrate and not be reflected at the boundary.

Figure 4.1 shows two ACP65-AW-GSG-250 probes connected to the coplanar line. For the ACP110-AW-GSG-100 probes, the connection of the probes is identical, only the coplanar line with different dimensions is used. The following Figure 4.2 shows a close-up view of both types of tip connected to the coplanar line, also showing how the substrate extends below the probe tips.

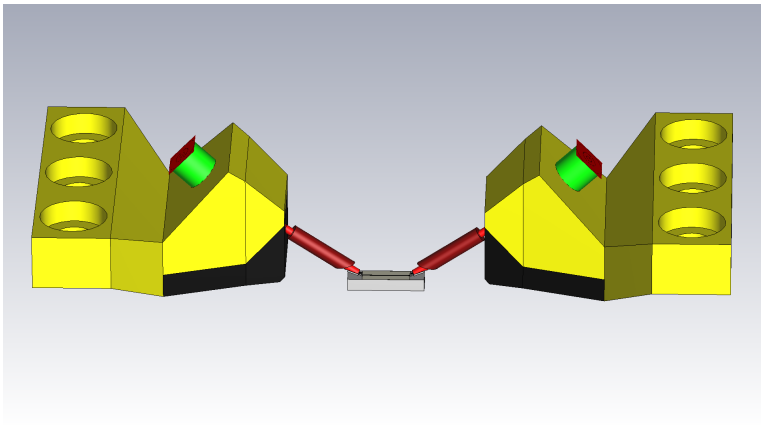

Figure 4.1. Simulation view of two ACP65-AW-GSG-250 probes connected to a coplanar line.

The simulations of both types of probes are set to the frequency range in which they operate, i.e. up to 65 GHz and 110 GHz respectively. As the probes are large relative to the wavelength, all materials are defined as lossless due to the complexity of the simulation. The conducting materials are set to PEC (perfect electric conductor), the

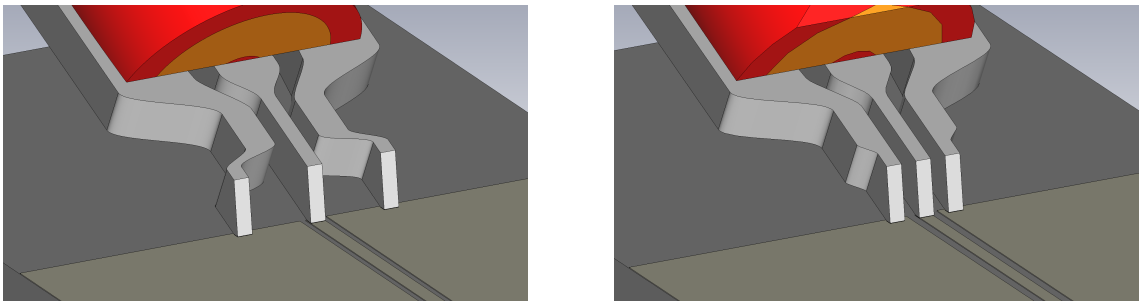

(a) (b)

Figure 4.2. Detailed view of the tip of the probe model (a) ACP65-AW-GSG-250, (b) ACP110-AW-GSG-100 connected to the coplanar line.

dielectric has zero loss, the absorbing material on the micro-coaxial line has vacuum properties, and the absorbing material of the probe body (the black part in 4.1) has relative permittivity $\epsilon_r = 3$.

4.1 Coplanar Waveguide

Alumina with relative permittivity $\epsilon_r = 10$ is used as the substrate of the coplanar conductor. Both versions are designed according to the control lines „through“ on a calibration substrate from FormFactor, Inc. The dimensions of both lines are given in the Table below 4.1.

Table 4.1. Table of coplanar line dimensions.

Pitch	Height of substrate	Width of signal line	Gap	Thickness
100	254 μm	45 μm	30 μm	3 μm
250	635 μm	50 μm	20 μm	3 μm

The substrate is longer than the plating at both ends to make the simulation as close to reality as possible. In a real measurement (e.g. calibration), part of the field is not coupled into the coplanar line and is radiated into the surroundings where it interacts with the ceramic substrate and causes losses.

4.2 Simulation Results

The resulting simulated S-parameters of both probes are shown in Figure4.3 and 4.4. Only the parameters S_{11} and S_{21} are shown here, due to symmetry S_{22} and S_{12} appear identical. This data shows that both models are functional. The reflection coefficient S_{11} is quite wavy in both cases, indicating the existence of resonances arising at discontinuities in the model. The S_{11} reaches relatively high values, worse than -5 dB at 65 GHz for the ACP65-AW-GSG-250 probe (Figure 4.4), and this is more than the real probe. The main reason for this is that all materials in the simulation are lossless. If the materials were considered with losses, the reflection coefficient would be smaller. At the same time, it is important to note that it is not possible to directly compare the parameters of a single probe from the manufacturer with those from the simulation, because it is more complex. The simulation is a cascade of a probe, a coplanar waveguide and another probe. It must have worse S-parameters because there are more

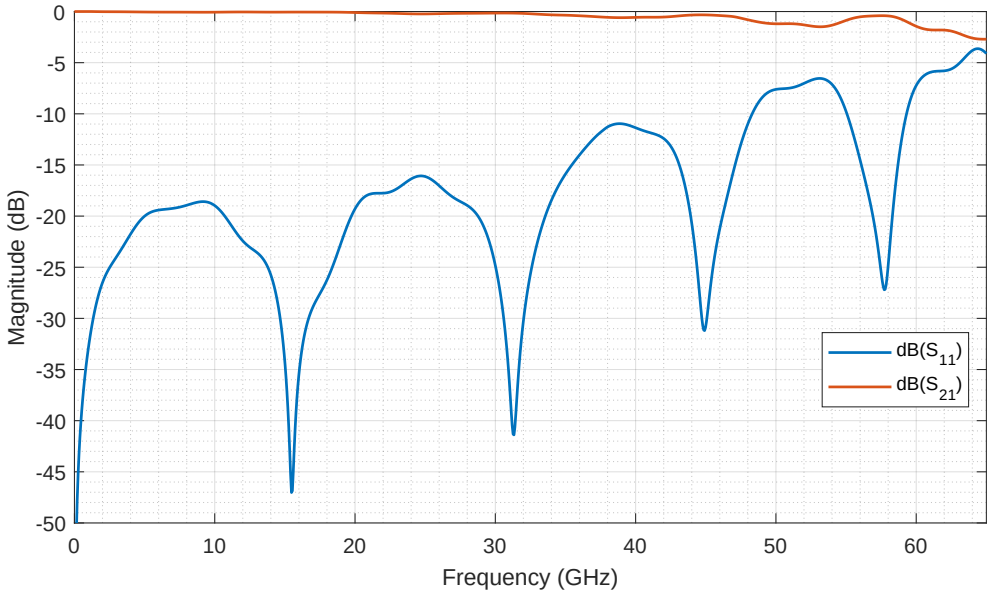

Figure 4.3. Simulated S-parameters of the ACP65-AW-GSG-250 probe.

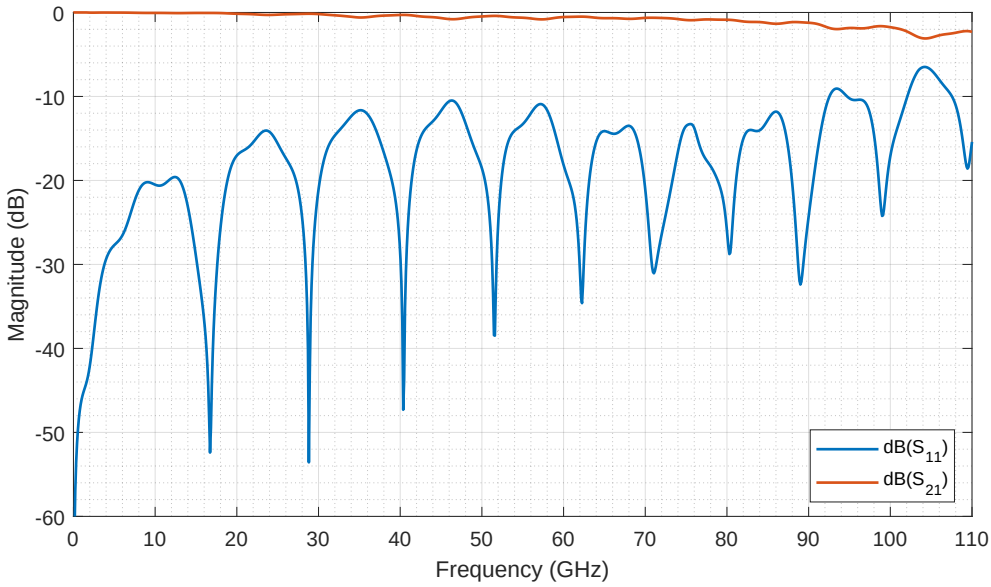

Figure 4.4. Simulated S-parameters of the ACP110-AW-GSG-100 probe.

discontinuities, so standing waves are more likely to appear. It is therefore logical that the S-parameters in the simulation will be different and worse than those given by the manufacturer for the probe itself.

Chapter 5
Calibration and Correction of Simulated Data

Since the purpose of this thesis is to obtain simulated data that are comparable to real measurement, it is necessary to follow the same steps as in real life. The two ports DUTs are characterised through the models of ACP probes. Only the probe tip and part of microcoaxial cable were used in the simulation (see Figure 5.1), because the whole body of the probe is significantly large, relatively to the wavelength, has hardly any impact on the simulated S-parameters, but would hugely impact the simulation time. As calibration method, UOSM (Unkonwn-Open-Short-Match) technique was opted for thanks to its great degree of accuracy and relative simplicity. Also, LRRM (Load-Reflect-Reflect-Match) method was considered, which is widely used for probe measurement due to its relative insensitivity to small errors in probe placement that are inherent in microwave probing [9]. However, in the case of simulations the probes can be always placed perfectly in the same position so this advantage becomes irrelevant.

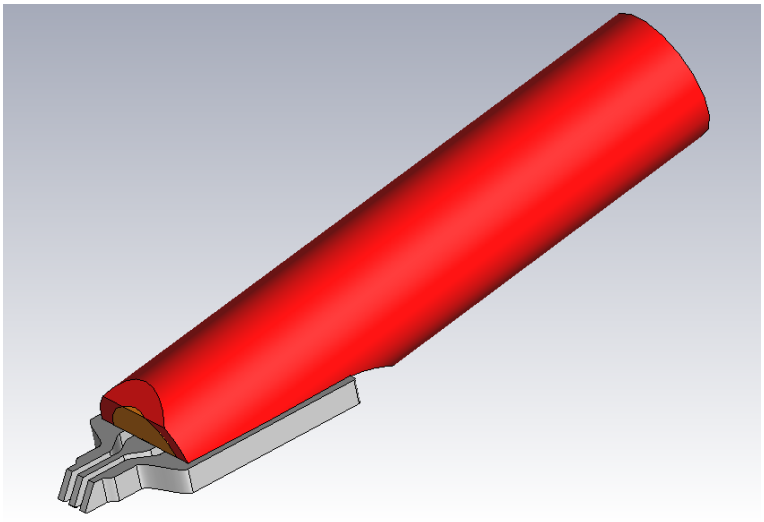

Figure 5.1. Part of the probe ACP110-AW-GSG-100 used for simulations.

5.1 Models of Calibration standards

Two error boxes are computed from UOSM calibration method using 7-term error model. S-parameters of three standards (open, short and match) and an unknown thru needed to be measured (simulation with two probes). These calibration standards, for probe ACP110-AW-GSG-100, were modelled according to the calibration standard substrate (FormFactor 104-783) manufactured by FormFactor, Inc. and simulated in CST Studio Suite. Afterwards their theoretical models, characterised by lumped elements with values of parameters stated by the vendor, were simulated in AWR Microwave Office.

5.1.1 Unknown Thru

This calibration standard is a simple coplanar waveguide defined by its dimensions in Table 5.1. Figure 5.2 displays 3D model in CST Studio Suite and also its idealised representation in AWR Microwave studio. In Figure 5.3 the simulated data measured by the probes are presented. On the left y-axis is shown S_{11} in dB and on the right axes is the transmission coefficient S_{21} also in dB. The S_{11} values are kept below -15 dB and the S_{21} is very high, which means that the unknown thru and the probes are well matched and behave as expected. This further confirms the linear phase of the transfer coefficient in the Figure 5.4.

Table 5.1. Dimensions of the calibration standard unknown thru.

Width of middle line	Gap	Length
45 μm	30 μm	200 μm

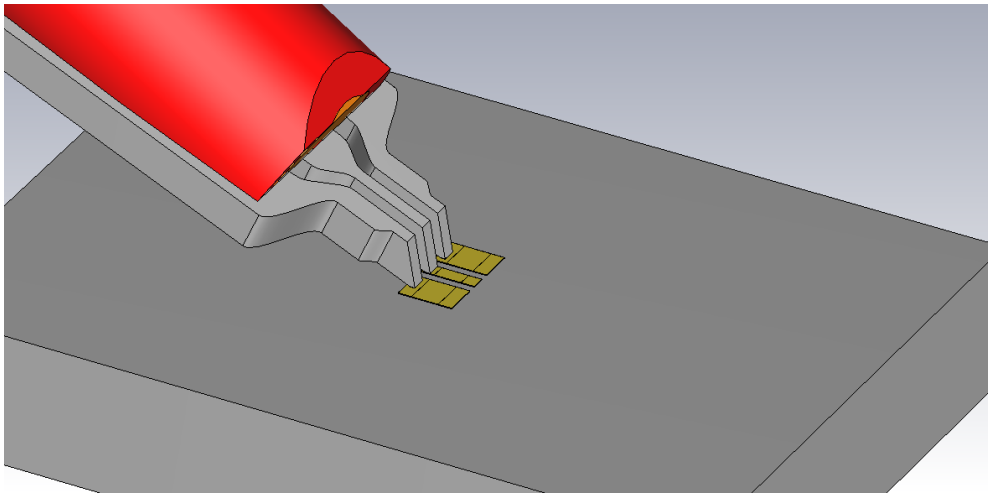

Figure 5.2. Calibration standard unknown thru with connected probe ACP110-AW-GSG-100.

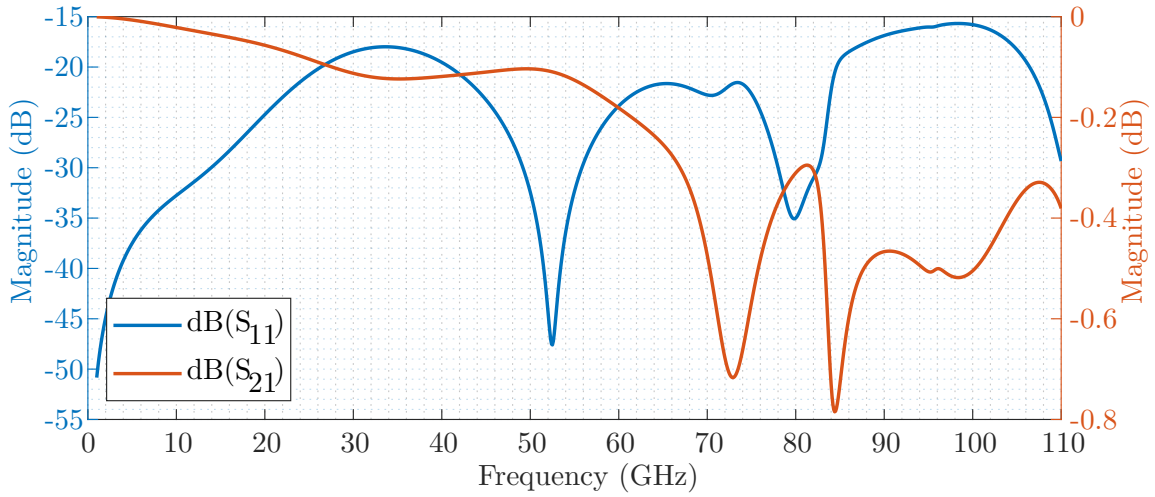

Figure 5.3. Measurement simulation of calibration standard thru measured by a probe ACP110-AW-GSG-100.

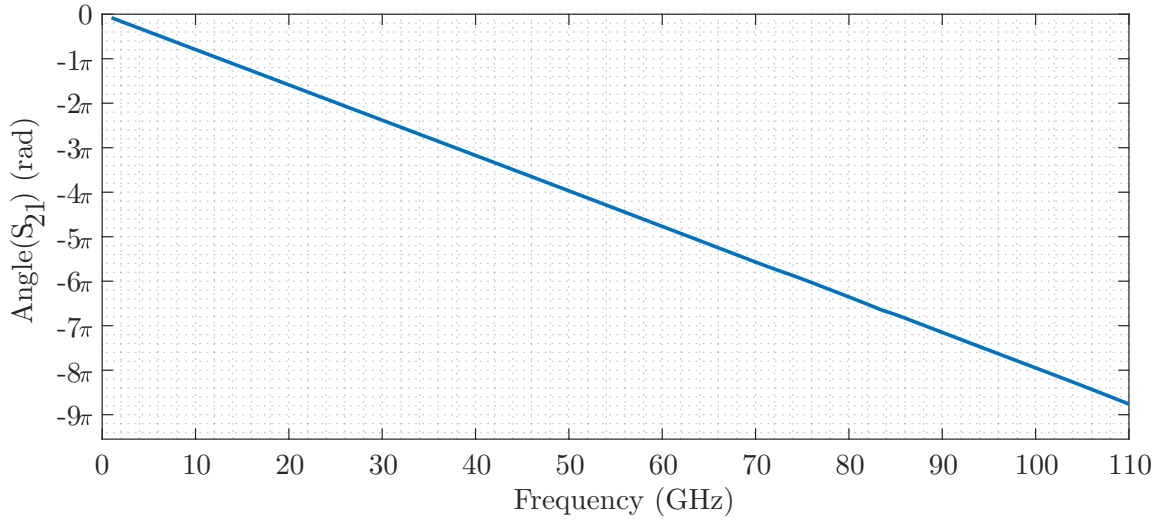

Figure 5.4. Unwrapped phase S_{21} of measurement simulation of calibration standard thru measured by a probe ACP110-AW-GSG-100.

5.1.2 Open

Calibration standard open is simply two probes lifted in the air in defined distance. Identically was simulated the calibration standard in this case. The probes are approximately 130 μm away from each other. The simulated S_{11} of calibration standard open are shown in the Figure 5.5. Here it can be observed that the S-parameters behave as expected. That is, very high reflection and phase starting at 0 degrees. The standard on its own is model as ideal -9.3 fF capacitor.

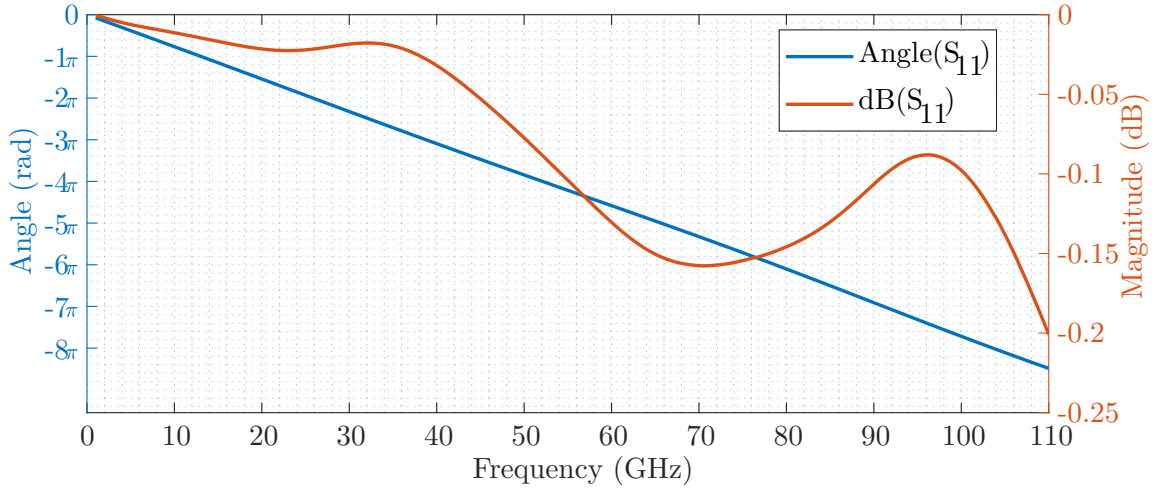

Figure 5.5. Measurement simulation of calibration standard open measured by a probe ACP110-AW-GSG-100.

5.1.3 Short

Short is naturally designed as thin metal plate connecting signal and both ground pins. In the Table 5.2 are mentioned its proportions. Figure 5.6 shows the 3D model of the short with a probe connected. Its simulated S_{11} in dB and its phase is pictured in the Figure 5.7. The reflection coefficient is again very high with a linear phase starting at pi, which are the results that were expected and confirm the validity of the simulation. It is characterised by 2.4 pH inductor in series.

Table 5.2. Dimensions of the calibration standard short.

Width	Length	Gap between the two shorts
350 μm	50 μm	100 μm

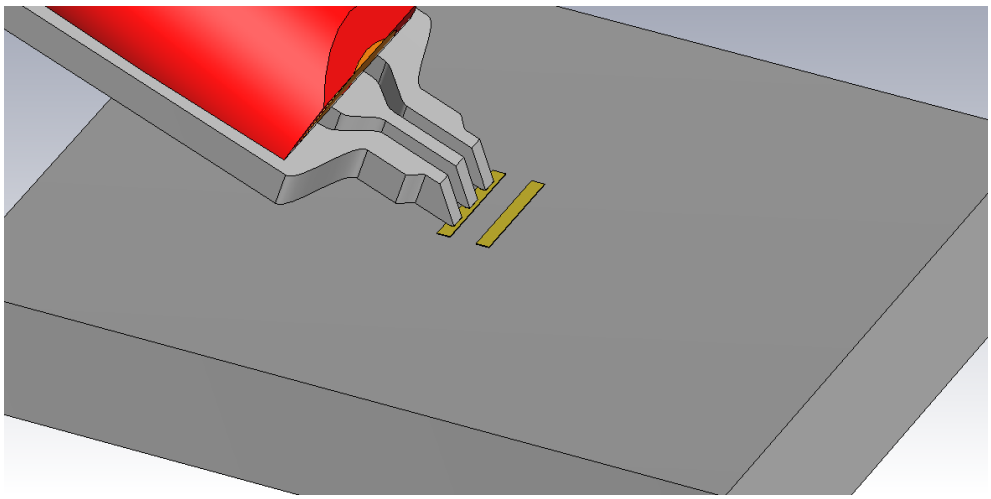

Figure 5.6. Calibration standard short with connected probe ACP110-AW-GSG-100.

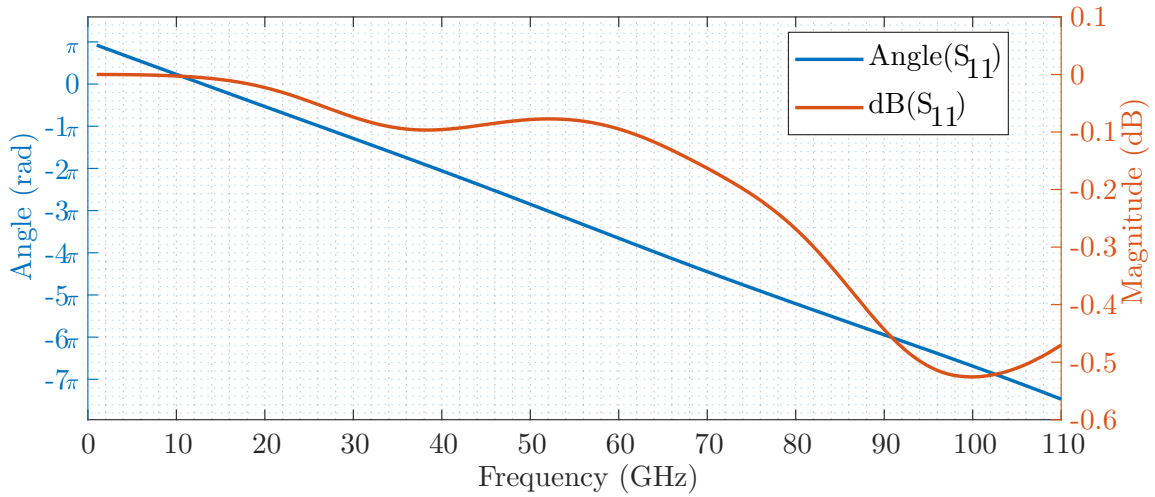

Figure 5.7. Measurement simulation of calibration standard short measured by a probe ACP110-AW-GSG-100.

5.1.4 Match

This calibration standard match is implemented as 50 Ω load connected to ground. Two 100 Ω resistors in parallel made up of resistive sheet material are placed between signal and ground strips on both sides. It has the same dimensions as the thru calibration standard (Table 5.1). In the Figure 5.9 are the simulated data measured by the probes. The S_{11} is kept below -15 dB, which shows well impedance matching. In addition to the 3D model, its equivalent circuit, consisting of 50 Ω resistor and -3.5 pH inductor in series, is shown in the Figure 5.8.

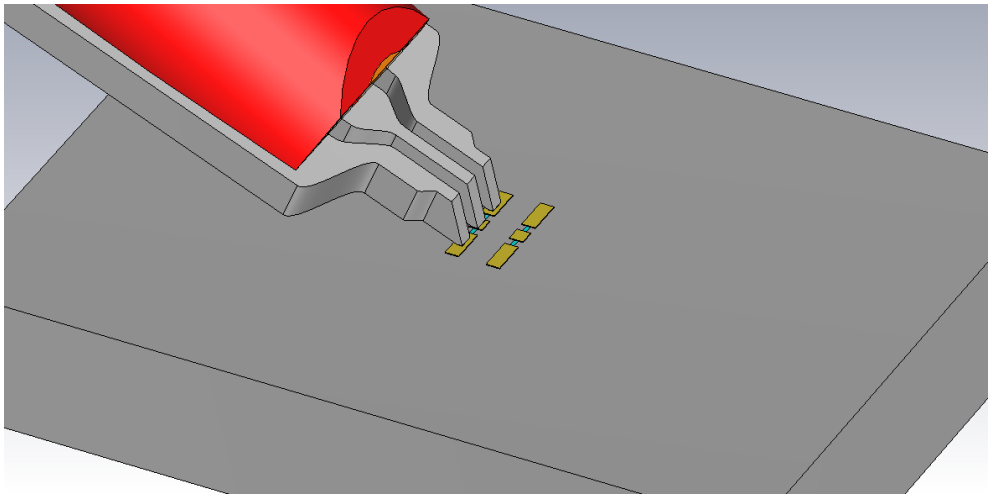

Figure 5.8. Calibration standard match with connected probe ACP110-AW-GSG-100.

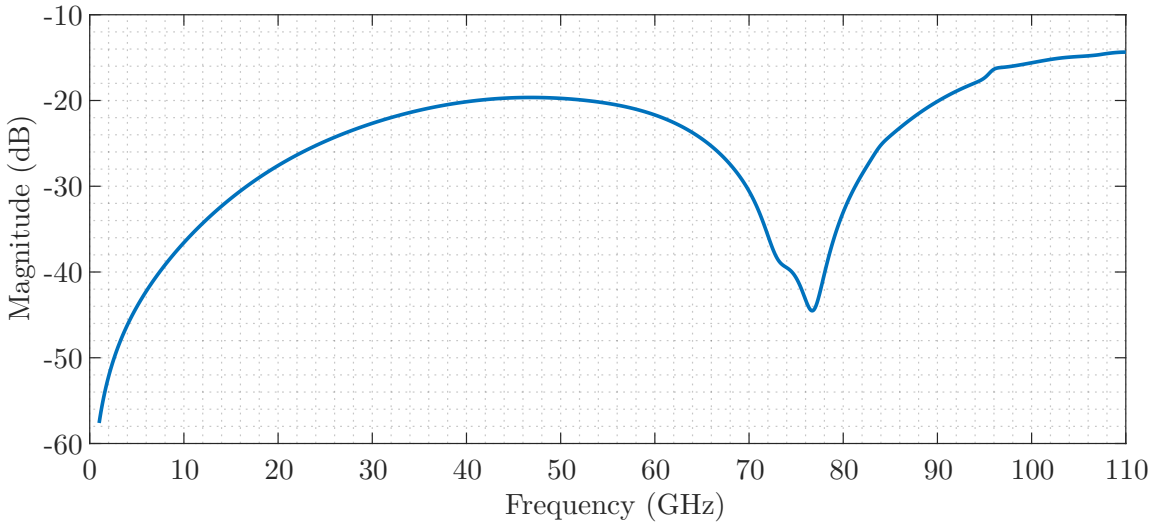

Figure 5.9. Simulated S_{11} magnitude in dB of the calibration standard match measured by a probe ACP110-AW-GSG-100.

5.2 Calibration Validation

The verification of the UOSM calibration was carried out using the same unknown through line as that used in the initial calibration process. However, the calibration does not directly use the thru standard to calculate the error boxes. It is only used to decide between two possible solutions. In the Figure 5.10 are depicted the raw simulated, corrected and ideal reflection coefficients in dB. It is clear that the UOSM calibration has successfully managed to remove the influence of the CPW probes, and the resulting data are very close to the ideal thru model. The verification involved comparing the phase of the ideal thru model with the measured one. The results presented in the Figure 5.11 showed that the maximum observed phase deviation was minimal, consistently in the range of single units of degree. Such a small deviation confirms the high accuracy of the calibration and indicates that the corrected measurements are highly reliable [10]. This level of accuracy is critical for applications such as de-embedding, because even small errors can cause unreasonable outcomes.

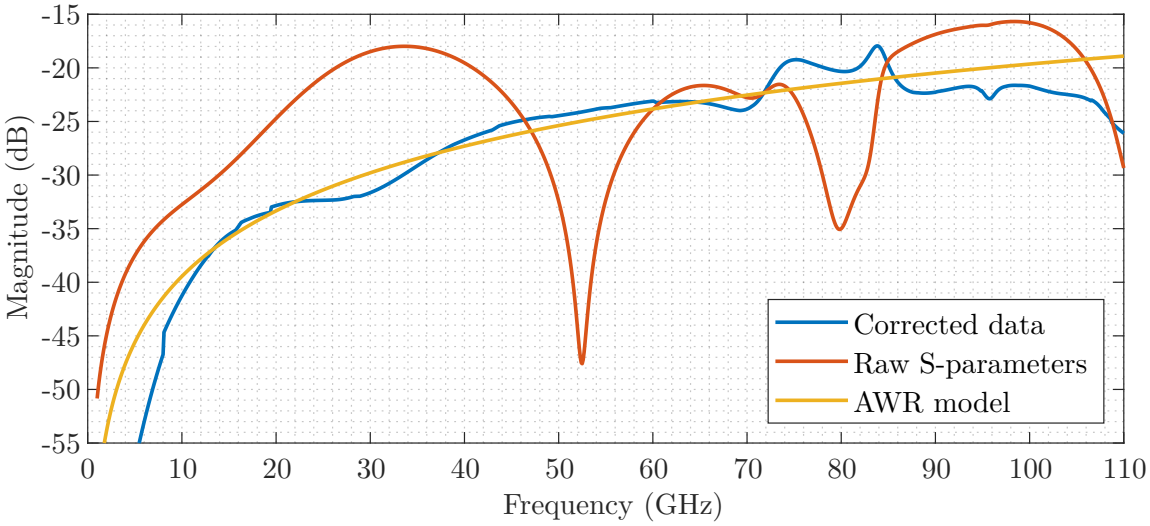

Figure 5.10. Comparison of unknown thru simulated S_{11} measured by a probe ACP110-AW-GSG-100.

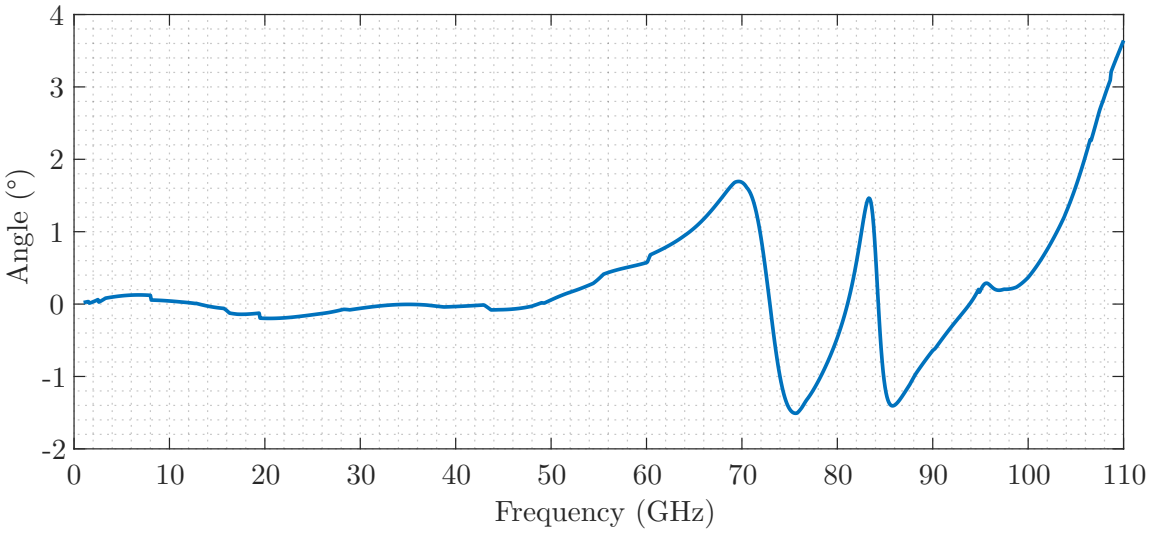

Figure 5.11. Maximal phase deviation of the transmission coefficient in degrees. Comparison of simulated measurement and ideal model of thru.

Chapter 6
De-Embedding

De-embedding is the process of deducing the impedance of a device under test from measurements made at a distance, when the electrical properties of the intervening structure are known [11]. It is a mathematical apparatus widely used for on-wafer measurement of integrated circuits, because it is often impossible to measure the characteristics of the DUT directly. The device is connected via transmission lines to the connecting pads (in other words is embedded in them), which are used to connect the measuring probes. So de-embedding mathematical algorithms are implemented to shift the reference plane to the DUT level. These techniques rely on the exact knowledge of the DUT and additional de-embedding structures [12]. In this thesis two methods based on three devices (OPEN, SHORT and THRU) were implemented and analysed: OPEN-SHORT and THRU.

Firstly, it is necessary to define two principal terms, RAW and DUT reference planes. By DUT it is meant only the functional device without any support structures, such as interconnections, feed lines and pads for on-wafer testing. The RAW device is whole physical device as it has been designed and measured on wafer. Unlike, calibration where exist sets of calibration standards, it is impossible to have standardised RAW devices. Every measured DUT is different and needs to be treated differently according to its electrical and geometrical properties. In the Figure 6.1 are examples of different devices. The necessity of RAW devices lies in the fact, that typically the DUT is much smaller than the coplanar probes used in the measurement. Designing the embedded DUT naturally leads to the de-embedding step [1].

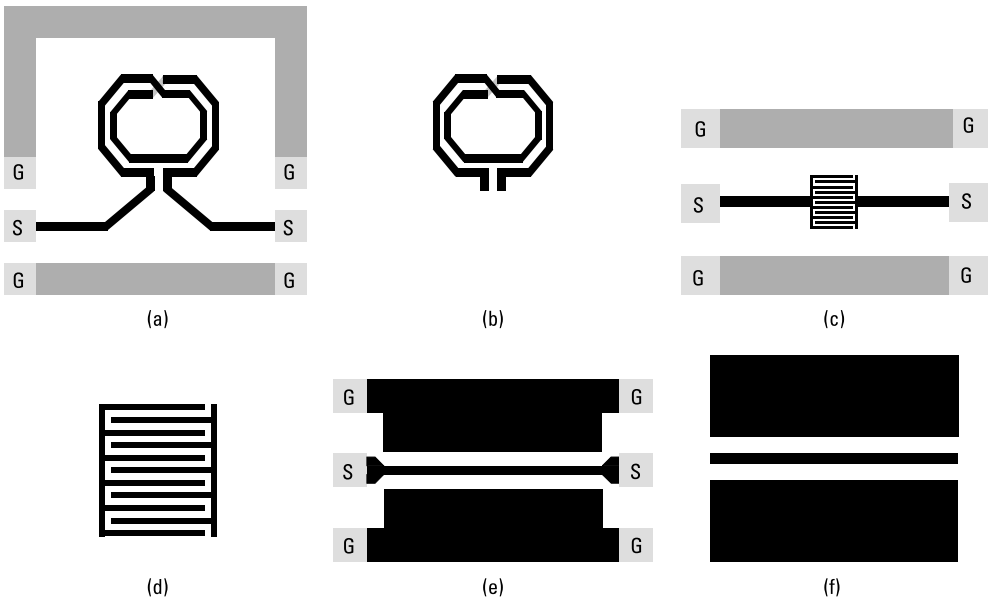

Figure 6.1. Examples of different structures for de-embedding. (a) RAW inductor, (b) Inductor DUT, (c) RAW MOM capacitor, (d) MOM capacitor DUT, (e) RAW CPW T-line, (f) CPW DUT. Source: [1]

All three techniques described in the following chapters are based on the representation of the DUT and its RAW test structure with an equivalent lumped element network [1]. First step is to design all necessary de-embedding structures (OPEN, SHORT, THRU) and measuring their S-parameters. Then the chosen algorithm is applied on the measured data, de-embedding the DUT from the RAW device. This procedure is suitable for measuring a large number of different types of DUTs with different layouts.

6.1 OPEN-SHORT De-Embedding

The OPEN-SHORT de-embedding approximates the parasitic characteristics of the RAW device by the equivalent lumped element network pictured in the Figure 6.2. The DUT is surrounded by impedance Z and admittance Y elements. The series inductance elements Z_{ser} represent the influence of resistance R and inductance L of the interconnecting transmissions. These also contribute parasitic capacitances, which are described by an admittance $Y_s = j\omega C$ [1].

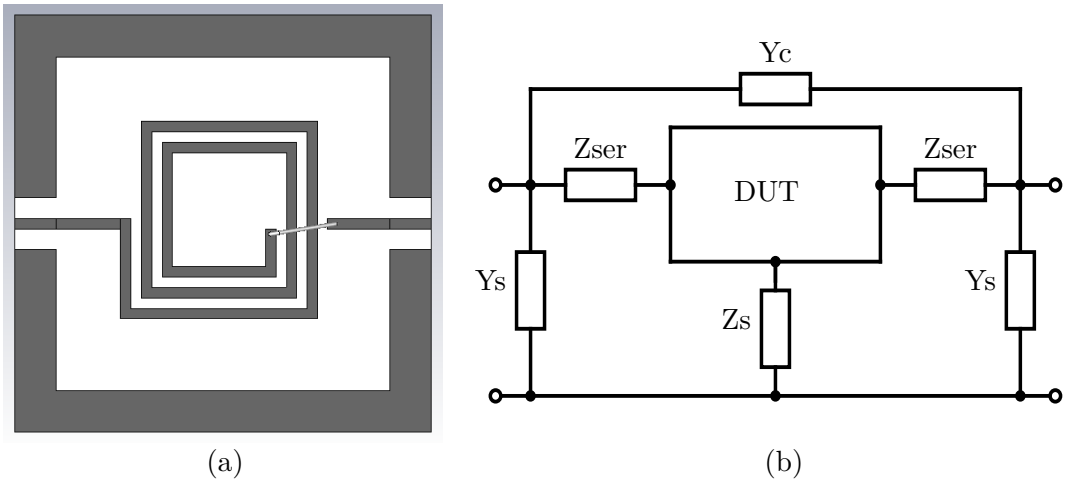

Figure 6.2. (a) RAW structure of an inductor, (b) OPEN-SHORT de-embedding equivalent lumped element network. Based on [1].

This method needs two additional structures OPEN and SHORT, which are both depicted in the Figure 6.3 with their corresponding equivalent networks. The open device is formed by removing the DUT and ensuring there is no conductive path between the two ports. The lumped element network is formed out of series admittance which stands for the capacitance coupling between the two terminals. Then the shunt capacitance is formed at the contact pads between the signal strip and the grounds. SHORT device is formed similarly as OPEN but the two ends of transmission lines are shorted to the ground. The unwanted characteristics are also similar to the OPEN, but in addition a series impedance Z_{ser} is present between the RF port and the ground.

After having explained the design procedure and meaning of the equivalent lumped element network, next step is to progress by introducing the mathematical formulation of this de-embedding technique. The method is adopted according to [1] and [13].

The input data are of course the measured S-parameters in the form of a 2×2 matrix,

$$S = \begin{bmatrix} S_{11}(f) & S_{12}(f) \\ S_{21}(f) & S_{22}(f) \end{bmatrix}, \tag{1}$$

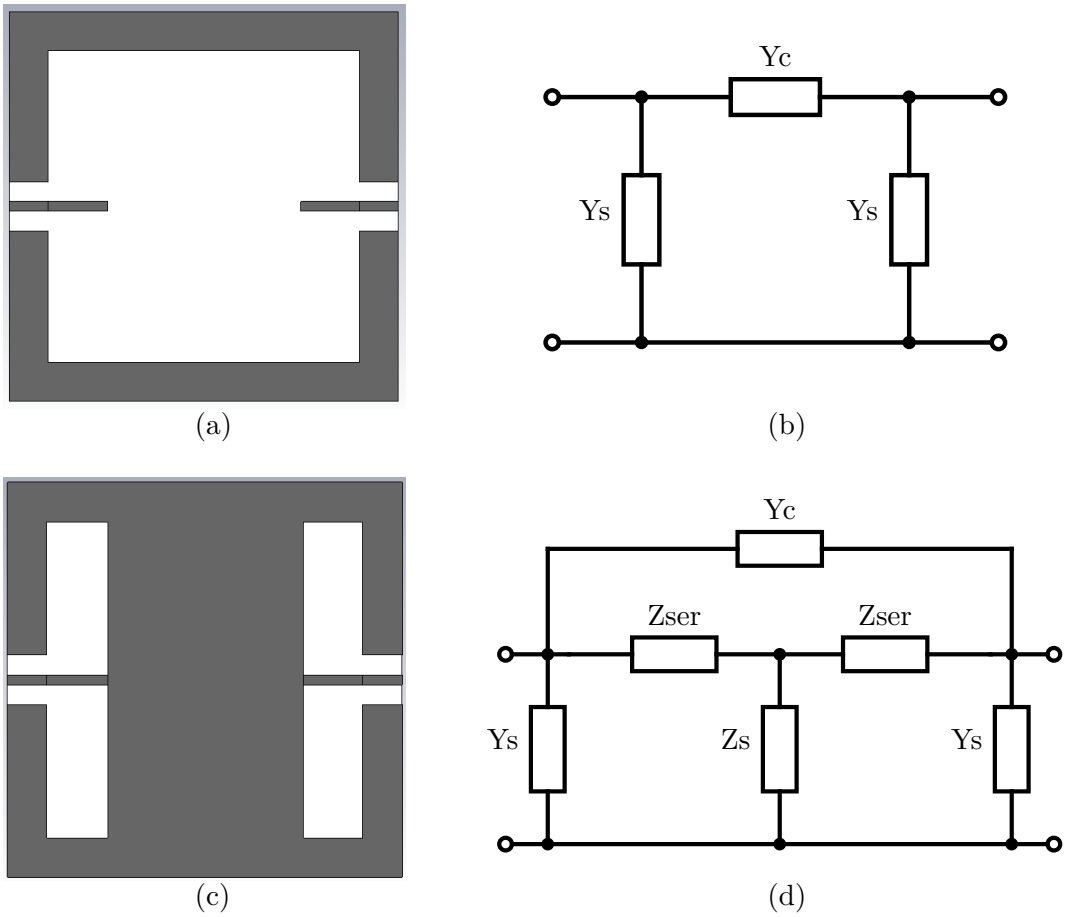

Figure 6.3. Required de-embedding structures. (a) OPEN device, (b) OPEN equivalent lumped element network, (c) SHORT device, (d) SHORT equivalent lumped element network. Based on [1].

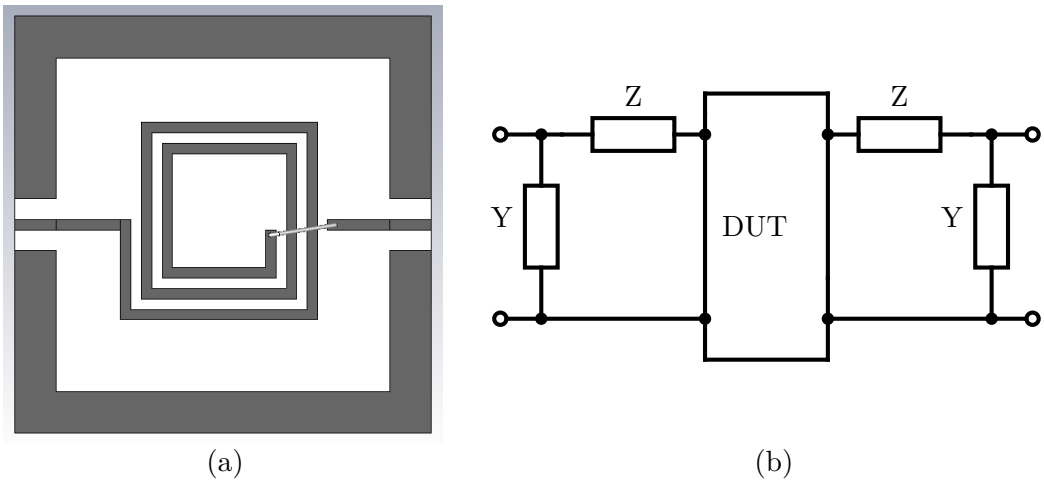

Figure 6.4. (a) RAW structure of an inductor, (b) THRU de-embedding equivalent lumped element network. Based on [1].

where the elements S_{ii} are frequency dependent, thus the whole matrix becomes multidimensional $2 \times 2 \times Nfreq$. $Nfreq$ is number of frequency points in which the measured network is characterised by a 2×2 S-parameter matrix. The algorithms take advantage of other equivalent multidimensional matrix representations with Y-, Z-, T-

and ABCD-parameters. OPEN-SHORT de-embedding technique uses simple algebraic matrix operations. In the first step the OPEN admittances are removed from the RAW device using Y-parameters,

$$Y_{RO} = Y_{RAW} - Y_{OPEN}, \tag{2}$$

where Y_{RAW} and Y_{OPEN} are the Y-matrices converted from measured S-parameters of the RAW and OPEN devices, respectively. Next step is to remove the OPEN capacitance from the SHORT device using analogous operation,

$$Y_{SO} = Y_{SHORT} - Y_{OPEN}, \tag{3}$$

where Y_{SHORT} is the Y-parameters matrix converted from the measured S-parameters. Following step is to convert both Y_{RO} and Y_{SO} to Z-parameters Z_{RO} and Z_{SO}. Finally, Z-matrix of the DUT is extracted by removing remaining series impedance by,

$$Z_{DUT} = Z_{RO} - Z_{SO}, \tag{4}$$

and converted back to S-parameters, which ideally represent the de-embedded S-parameters of the DUT itself. The implemented method as a MATLAB script is attached in the Appendix A.

From the mathematical point of view the de-embedding algorithm is solid and allows for a perfect extraction of the DUT from RAW device [1]. Nevertheless, in real-world design it is crucial to mention that the OPEN-SHORT technique will perform only as good as the proper OPEN and SHORT devices are designed [14].

6.2 THRU De-Embedding

Regardless of the number of devices that need to be designed, the THRU method is simpler and more efficient, thus time saving also silicon area and costs. It is based on the same principles as the previous technique OPEN-SHORT. The parasitic characteristics are derived from the RAW device called THRU and approximated by an equivalent lumped element network pictured in Figure 6.5. It consists of series impedance $Z = R + j\omega L$ of the leading structures and shunt admittance $Y = j\omega C$ between the ground and signal connecting pads. The design of the THRU structure is derived from the RAW device without the DUT. Then the open transmission lines are connected the shortest way possible. Important point is, that the THRU method assumes the thru connection to be ideally of zero electrical length with zero losses. In practice this is not achievable without modification to the whole device. For instances where the two terminals are opposite to each other, the whole GSG box should be shrunken and the two lead segments joined together. The thru must be symmetric and its symmetry plane should reflect exactly the DUT reference plane [1]. If this condition is not met it results in lower accuracy of the de-embedded data and even failure of the whole method.

First step of the actual de-embedding algorithm is to express the RAW device as a cascade of T-parameter matrices of the following form,

$$T_{RAW} = T_{LEFT} \times T_{DUT} \times T_{RIGHT}\,, \tag{5}$$

where T_{RAW} are T-parameters converted from measured S-parameters, T_{LEFT} and T_{RIGHT} are T-matrices that represent the influence of the lead transmission lines and T_{DUT} are T-parameters of only the DUT itself. In Figure 6.4 is depicted the thru

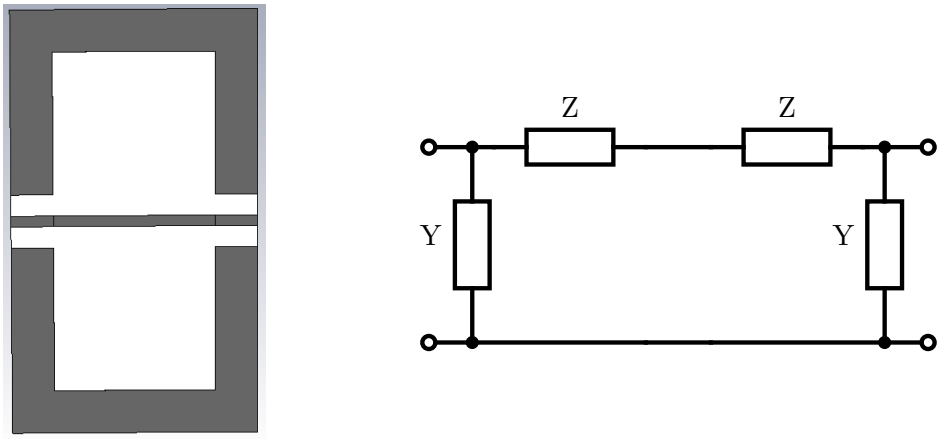

(a) (b)

Figure 6.5. (a) THRU structure, (b) THRU equivalent lumped element network. Based on [1].

device and its equivalent lumped element network. In comparison with the network of the RAW device (Figure 6.5) it can be easily identified that the THRU device is represented only by the parasitic characteristics of the two leading lines,

$$T_{THRU} = T_{LEFT} \times T_{RIGHT}\,. \tag{6}$$

Each lead network is again represented by a series impedance Z and shunt admittance Y. To acquire the T-matrices of the left and right leading lines Y-parameters of the THRU device are used,

$$Y = \begin{bmatrix} Y_{11} & Y_{12} \\ Y_{21} & Y_{22} \end{bmatrix}, \tag{7}$$

from which the Y-matrices of the leading lines are,

$$Y_{LEFT} = \begin{bmatrix} Y_{11} - Y_{12} & Y_{12} \\ 2Y_{12} & -Y_{12} \end{bmatrix}, \tag{8}$$

and,

$$Y_{RIGHT} = \begin{bmatrix} -Y_{12} & Y_{12} \\ 2Y_{12} & Y_{11} - Y_{12} \end{bmatrix}. \tag{9}$$

Then the resulting Y-parameters are converted to T-parameters T_{LEFT} and T_{RIGHT} and used to calculate the final T-parameters of the DUT,

$$T_{DUT} = T_{LEFT}^{-1} \times T_{RAW} \times T_{RIGHT}^{-1}\,. \tag{10}$$

Last step is to convert T_{DUT} to S-parameters. The THRU de-embedding is simple and effective method compared to the others. On the other side, its accuracy heavily depends on the quality of the THRU device.

Chapter 7
Design of Simulated DUTs

Both the inductor and capacitor are planar CPW devices designed on a single-layer alumina substrate. Their dimensions have been carefully designed to ensure that the final products can be produced using conventional thin-film technology, which introduces a significant limitation. According to Cicor, the minimum dimensions for standard planar lines and gaps are 50 μm [15]. Taking this constraint into account, both devices have been designed to operate up to the highest possible frequency achievable within these dimensional limits. This approach ensures that the designs are not only feasible for current manufacturing processes but also optimized for high-frequency performance within the specified constraints.

7.1 Inductor

Designing a planar inductor that operates up to the tens of gigahertz with the highest possible Q factor would take a whole thesis. The primary factors influencing the design include core diameter, gap between lines, conductor width, and number of turns [16]. Given that the widths of lines and gaps are constrained by manufacturing limits to 50 m, the design possibilities were significantly restricted. The goal was to create an inductor that maintains inductive behaviour up to at least 20 GHz. AWR Microwave Studio was utilised to develop the initial proportions of the inductor, allowing for detailed electromagnetic simulation and optimisation. The design process involved iterating on the geometry to minimise parasitic effects such as capacitance and resistance, which are critical at high frequencies. The final physical parameters, optimised within the given constraints, are summarised in Table 7.1.

Table 7.1. Design parameters of the simulated inductor.

Width & Gap	Linear segments	Outer length	Lead lines length
50 μm	7	328 μm	270 μm

7.1.1 RAW

For the design of the RAW de-embedding model of a CPW inductor, a layout from AWR Microwave Office in the form of a Gerber file was utilized. The process began with defining the substrate, including contact pads and a ground plane to establish the fundamental structural elements necessary for accurate simulation. Once the substrate and its associated components were set up, the Gerber layout was imported and precisely aligned in the centre of the substrate to ensure that the transmission lines on both sides are the same.

The next step involved defining the leading transmission lines, which are critical for connecting the central signal pad to the inductor itself. These transmission lines

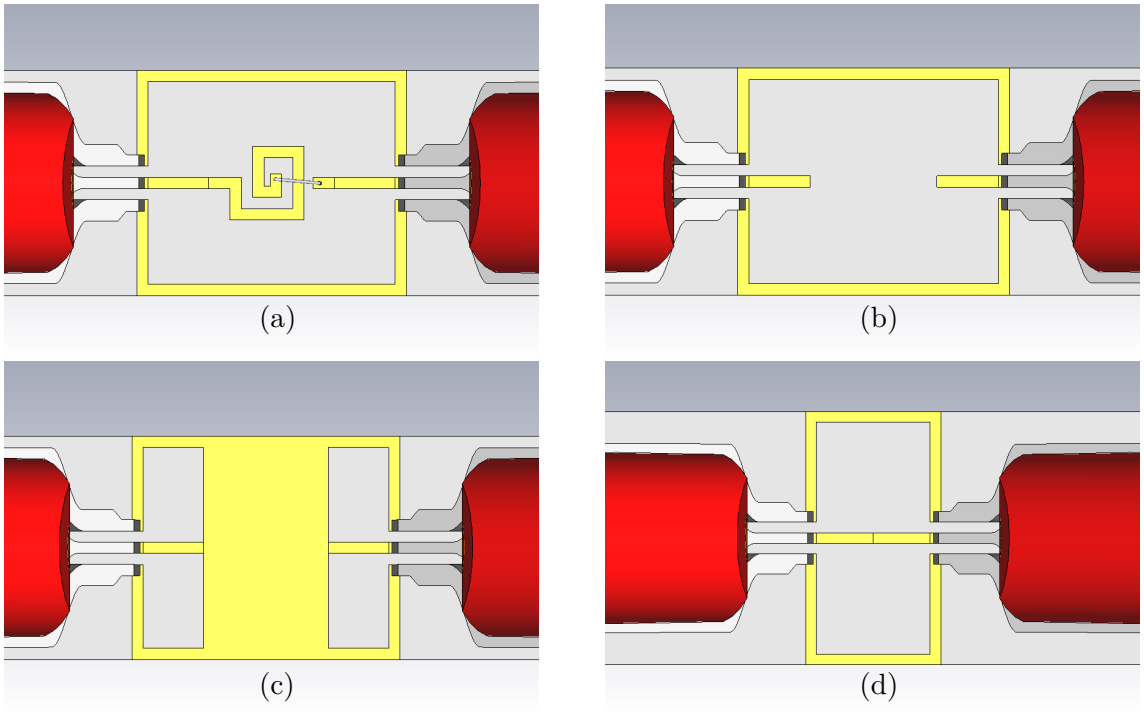

Figure 7.1. Designed inductor models of devices for OPEN-SHORT and THRU de-embedding with connected probes CP110-AW-GSG-100. (a) RAW, (b) OPEN, (c) SHORT and (d) THRU.

ensure that the signal can effectively reach the inductor while maintaining the integrity of the CPW design. Additionally, due to the use of a single-layer technology, it was necessary to define a bond wire to connect the inner end of the inductor to one of the side contact pads. This bond wire is essential for completing the circuit, given the single-layer constraint, and accurately represents the electrical connections in the physical inductor. The final device is presented in the Figure 7.1 (a).

7.1.2 OPEN

The OPEN de-embedding structure is an essential component of the de-embedding process, derived directly from the RAW device layout by omitting the DUT, in this case, the inductor. This way the two lines connecting the inductor and the contact pads stay open, meaning not being connected anywhere. The critical aspect of this approach is the preservation of the entire layout configuration—excluding the inductor—to ensure the OPEN's parameters mirror the parasitic contribution of the RAW. This setup is crucial for accurately isolating and characterizing the parasitic elements that influence the performance of the inductor and is pictured in the Figure 7.1 (b).

7.1.3 SHORT

The SHORT de-embedding structure forms a critical counterpart to the OPEN structure in the calibration process. It is derived from the RAW layout, like the OPEN, but instead of leaving the transmission lines open, they are directly connected to the ground at the reference plane. Initially, it may seem advantageous to move the ground, which is parallel to the transmission line, closer together to improve reflection at higher frequencies. However, this approach can lead to undesirable effects. While it indeed shortens the path of the current, leading to stronger reflections, the current in the

ground plane flows in the opposite direction compared to the one in the leading line. This opposite current flow introduces a negative mutual inductance, which, in turn, reduces the effective inductance of the SHORT structure. Consequently, this can cause an inductance offset in the measurements after de-embedding [17]. Therefore in the design the parallel ground wasn't moved as can be seen in the Figure 7.1 (c).

7.1.4 THRU

The THRU de-embedding structure represents last device in the process and is also derived from the RAW device layout. Again, the construction of the THRU begins by excluding the device under test. Subsequently, the two ends of the primary transmission lines, which would normally connect to the DUT, are linked to each other. For THRU de-embedding to be effective, it is crucial that this connection is as close to being lossless as possible and that its electrical length approaches zero. In scenarios where the two contact pads are positioned directly opposite to each other, achieving an ideal THRU structure can be straightforwardly accomplished by completely removing the section where the DUT was and directly connecting the transmission lines without any additional length. This ensures the ideal thru connection. The whole structure is presented in the Figure 7.1 (d).

7.2 Capacitor

The same requirements and constraints apply to the design of a capacitor as for an inductor. The lines and gaps can be only 50 μm wide, which severely limits the geometrical possibilities. The goal is to design a capacitor that works to the highest possible frequency, so the de-embedding techniques can be tested properly. Achieving this involves balancing the minimisation of parasitic inductance and resistance while ensuring structural integrity and manufacturability within the given dimensions. An advanced simulation and design tool AWR Microwave Office was used for the layout design of the capacitor. Final design parameters are summarized in the Table 7.2. Then the necessary support structures were designed in CST Studio Suite (Figure 7.2) and simulated afterwards.

Table 7.2. Design parameters of the simulated capacitor.

Width & Gap	Number of elements	Width	Length
50 μm	4	350 μm	400 μm

7.3 Reference Devices

To accurately compare the resulting S-parameters obtained through the de-embedding method, it was essential to simulate the S-parameters of the DUT itself. This posed a significant challenge because the used coplanar technology was not grounded, preventing the DUT from being excited as a traditional microstrip line. Consequently, a reference structure was designed, based on the RAW device but with modifications to overcome this challenge. Specifically, the reference structure was fed through a CPW transmission line, with the DUT connected to an extended signal strip. This configuration allowed for proper excitation and simulation of the DUT. By subsequently shifting the reference

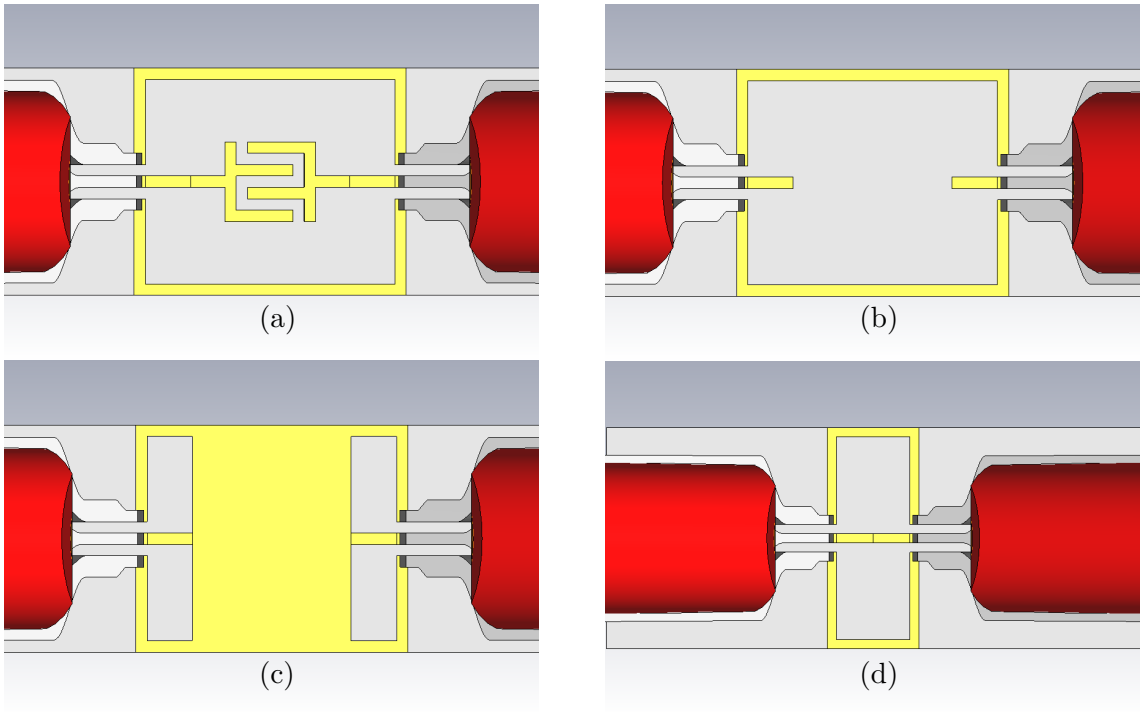

Figure 7.2. Designed capacitor models of devices for OPEN-SHORT and THRU de-embedding with connected probes CP110-AW-GSG-100. (a) RAW, (b) OPEN, (c) SHORT and (d) THRU.

plane along the homogeneous CPW transmission line to its end, the S-parameters of the DUT with a short leading line could be obtained. This process ensured that the comparison of S-parameters reflected the true performance of the DUT, free from the influence of the surrounding measurement setup.

7.3.1 Reference Inductor

In Figure 7.3 (a), the reference inductor designed for comparison with the de-embedded data is displayed. The reference planes of the simulation are positioned at the ends of the CPW, 0.95 μm from the inductor, as indicated by the dashed lines. This ensures that the measured S-parameters have matched reference planes to the de-embedding devices. By aligning the reference planes in this manner, the electrical characteristics of the inductor can be isolated, ensuring that the comparison reflects the DUT's performance rather than artifacts introduced by the measurement setup.

7.3.2 Reference Capacitor

Following the analysis of the inductor, the same procedure was applied to the capacitor, as shown in the Figure 7.3 (b). The capacitor, like the inductor, was designed with reference planes positioned at the ends of the CPW transmission lines (150 μm from the capacitor) to ensure consistency with the de-embedding structures. This again ensures reliable comparison between the true electrical performance of the capacitor and obtained S-parameters from the de-embedding methods.

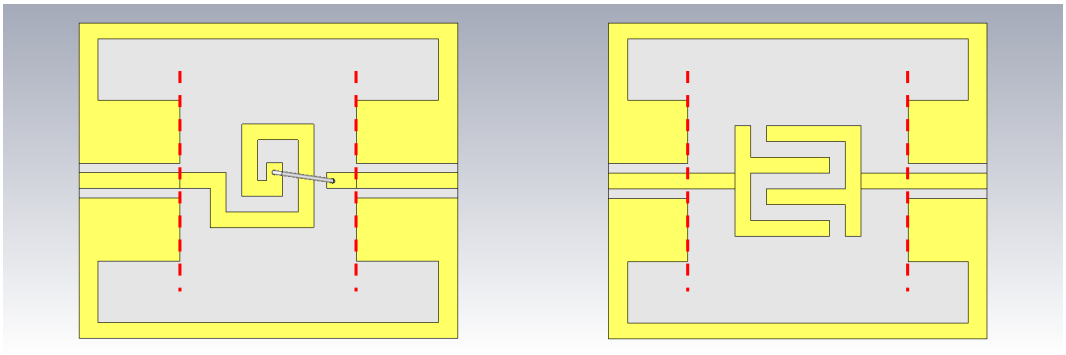

(a) (b)

Figure 7.3. Models of reference DUTs. Dashed lines indicate measurement reference planes. (a) Reference inductor, (b) Reference Capacitor.

Chapter 8
Results of Implemented De-Embedding Methods

Testing the de-embedding methods OPEN-SHORT and THRU was conducted using simulated models of an inductor and capacitor in CST Studio Suite designed on an alumina substrate. The structures were measured in the simulation by coplanar waveguide probes. Initially, it was essential to employ UOSM calibration to shift the reference plane to the tips of the probes, ensuring that the measurement reference plane was accurately positioned at the point of contact with the device under test. Following this calibration, the OPEN-SHORT and THRU de-embedding techniques were applied, using functions implemented in this thesis (see Appendix A and B) according to [1]. This process involved removing the effects of the parasitic elements introduced by the necessary supporting structures, thereby isolating the characteristics of the inductor and capacitor. The use of these de-embedding methods allowed for evaluation of the high-frequency performance of the components, validating the accuracy of the simulated models and ensuring the reliability of the measurement setup in capturing the true electrical behaviour of the devices.

8.1 UOSM Calibration

UOSM (Unknown Thru, Open, Short, Match) calibration is a versatile technique used in this thesis to calibrate simulated measurements in CST Studio Suite, specifically for simulations involving coplanar waveguide probes. This method requires four standards: an unknown thru connection, an open circuit, a short circuit, and a matched load (50 Ω). The primary inputs for UOSM calibration are the simulated S-parameters of these four standards. The calibration process uses these measurements to determine the error boxes associated with the simulation setup. In practice, UOSM calibration is applied by first simulating the response of each standard with the CPW probes in CST, then using the calibration algorithm to calculate the error boxes and then applying then on the measured data. This moves the reference plane to the desired location, such as the tips of the CPW probes in the simulation environment.

8.2 Inductor

When interpreting the de-embedded data of the inductor, it becomes evident that the OPEN-SHORT and THRU methods do not perform as expected. Figure 8.1 displays the magnitude of S_{11} (in dB) in the upper graph and the phase of S_{11} in the lower graph. The blue trace corresponds to the reference inductor discussed in Section 7.3.1, with the same reference plane as the OPEN-SHORT and THRU de-embedded data, represented by the orange and yellow traces, respectively. The purple dashed line represents the RAW inductor before de-embedding. It can be observed that up to approximately 20 GHz, the OPEN-SHORT and THRU methods somewhat follow the

reference trace. However, beyond 20 GHz, the de-embedded data diverges from the reference measurement, though not to an extent that suggests a complete failure or unrealistic results. Notably, above 50 GHz, the THRU data show $|S_{11}|$ values exceeding 0 dB, which is impossible for a passive device, as it implies signal amplification. The phase graph indicates that until 75 GHz, there is no unreasonable phase change that would suggest incorrect implementation of the methods.

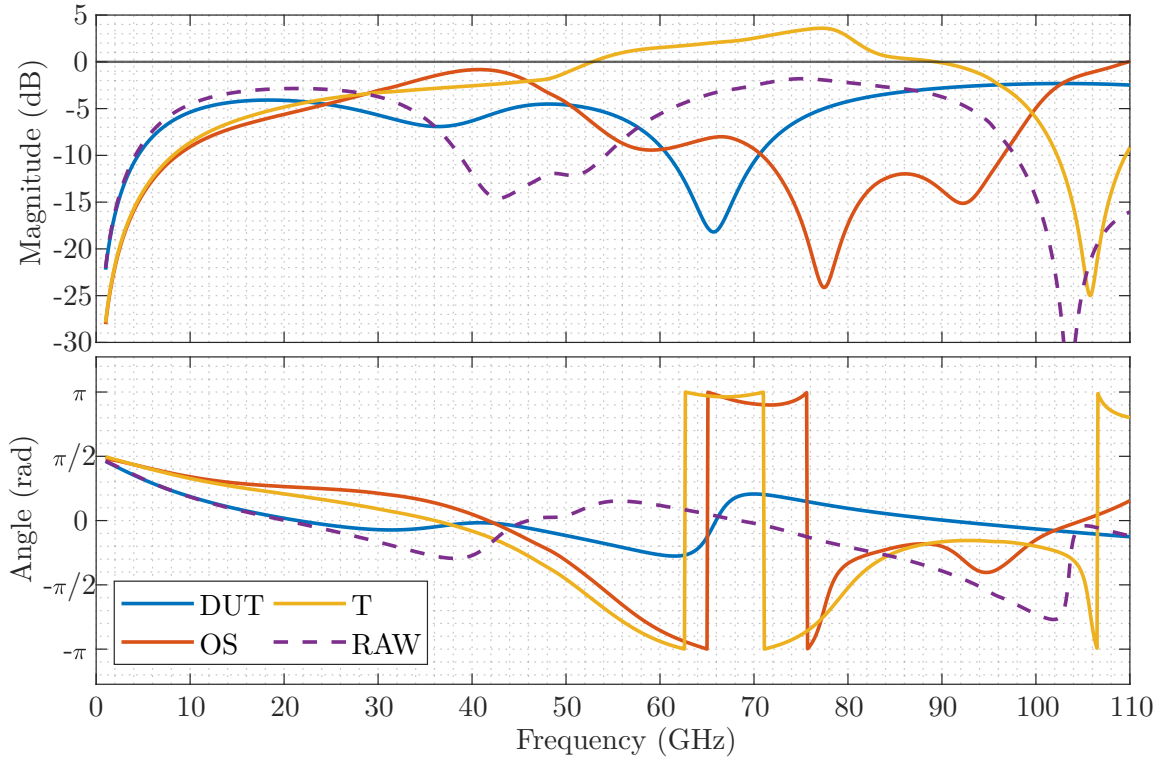

Figure 8.1. Inductor's S_{11} parameters obtained by OPEN-SHORT and THRU de-embedding compared with RAW device and simulated DUT. The upper image is the magnitude in dB, the lower image is the phase in rad.

In the second Figure 8.2, a similar trend is observed. At lower frequencies, the de-embedded data follow the reference inductor's transmission coefficient, but above 5 GHz, they again diverge and show results that cannot be considered consistent with the reference. Specifically, above 30 and 45 GHz, the magnitude of S_{21} surpasses the 0 dB line, indicating unrealistic results. However, the phase graph suggests that the methods are not incorrectly implemented, as there is no significant phase anomaly that would indicate fundamental errors in the de-embedding process.

8.3 Capacitor

At first glance, the de-embedded data for the capacitor appear more accurate than those for the inductor. Up to 15 GHz, the OPEN-SHORT and THRU methods closely follow the reference capacitor's data. However, beyond this frequency, the results become unreliable. Notably, the phase of the reflection coefficient does not indicate any errors in the de-embedding process itself. This suggests that while the de-embedding methods are correctly implemented, their effectiveness is constrained by the dimensions and properties of the DUT and the supporting structures, similar to the issues observed with the inductor.

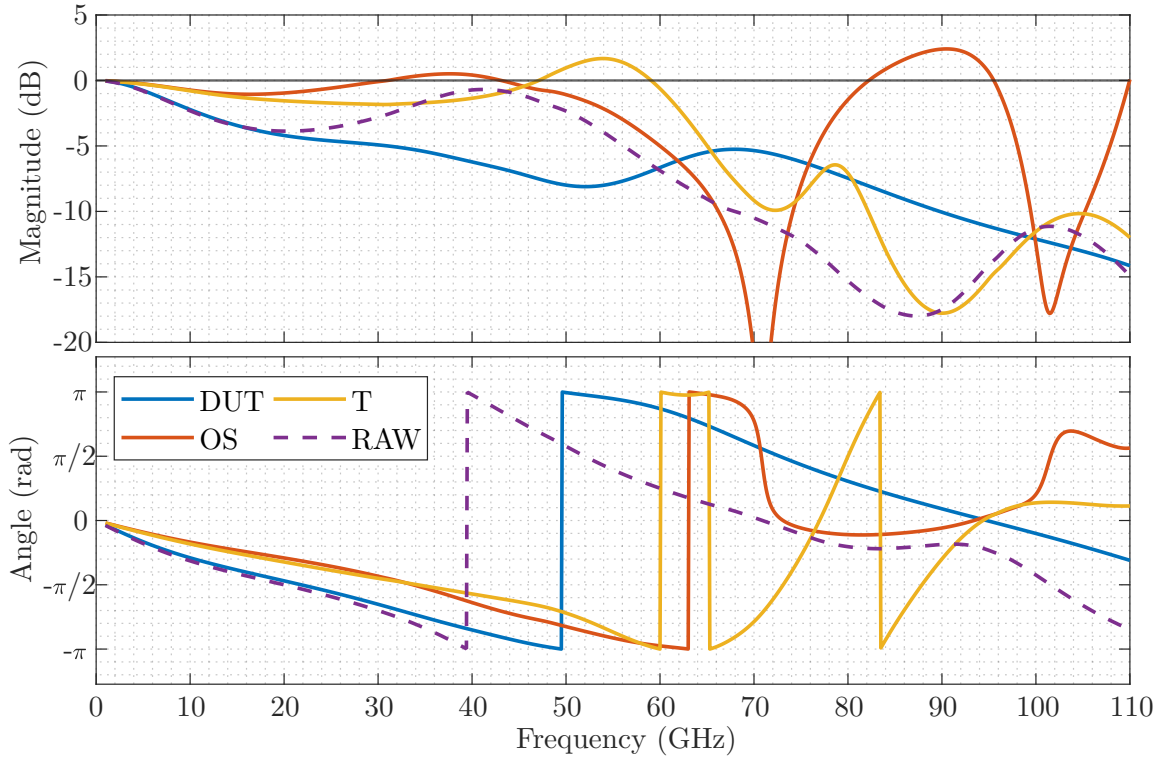

Figure 8.2. Inductor's S_{21} parameters obtained by OPEN-SHORT and THRU de-embedding compared with RAW device and simulated DUT. The upper image is the magnitude in dB, the lower image is the phase in rad.

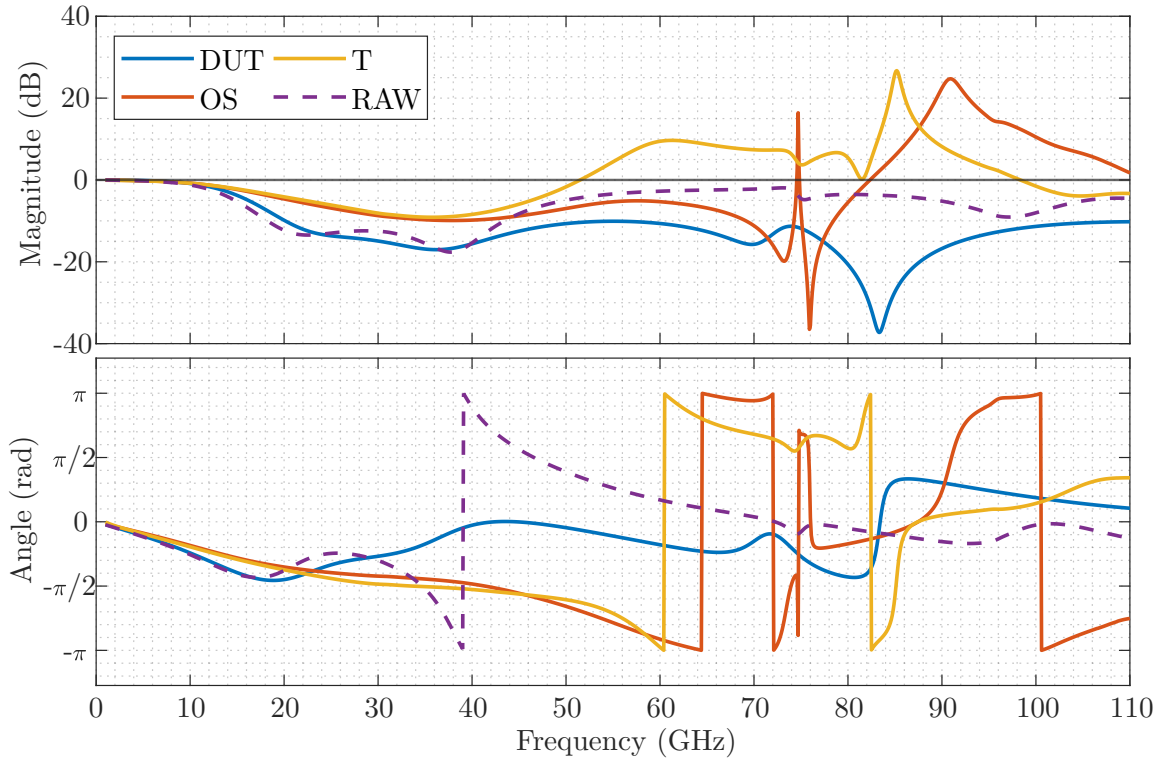

Figure 8.3. Capacitor's S_{11} parameters obtained by OPEN-SHORT and THRU de-embedding compared with RAW device and simulated DUT. The upper image is the magnitude in dB, the lower image is the phase in rad.

The trace of the transmission coefficient confirms that the de-embedding methods yield more accurate results for the capacitor than for the inductor. As shown in Figure 8.4, up to 20 GHz, the de-embedded data align more closely with the reference capacitor than the RAW device, indicating that the de-embedding process is isolating the DUT's characteristics within this frequency range. However, beyond the 20 GHz threshold, the traces begin to diverge significantly from the reference data, indicating that the de-embedding methods are less effective at higher frequencies, which is obvious. This divergence results in unreliable results, highlighting the limitations of the current de-embedding techniques when applied to planar devices with larger dimensions or at higher frequencies. Despite these limitations, again the phase data do not indicate fundamental errors in the implementation of the de-embedding process.

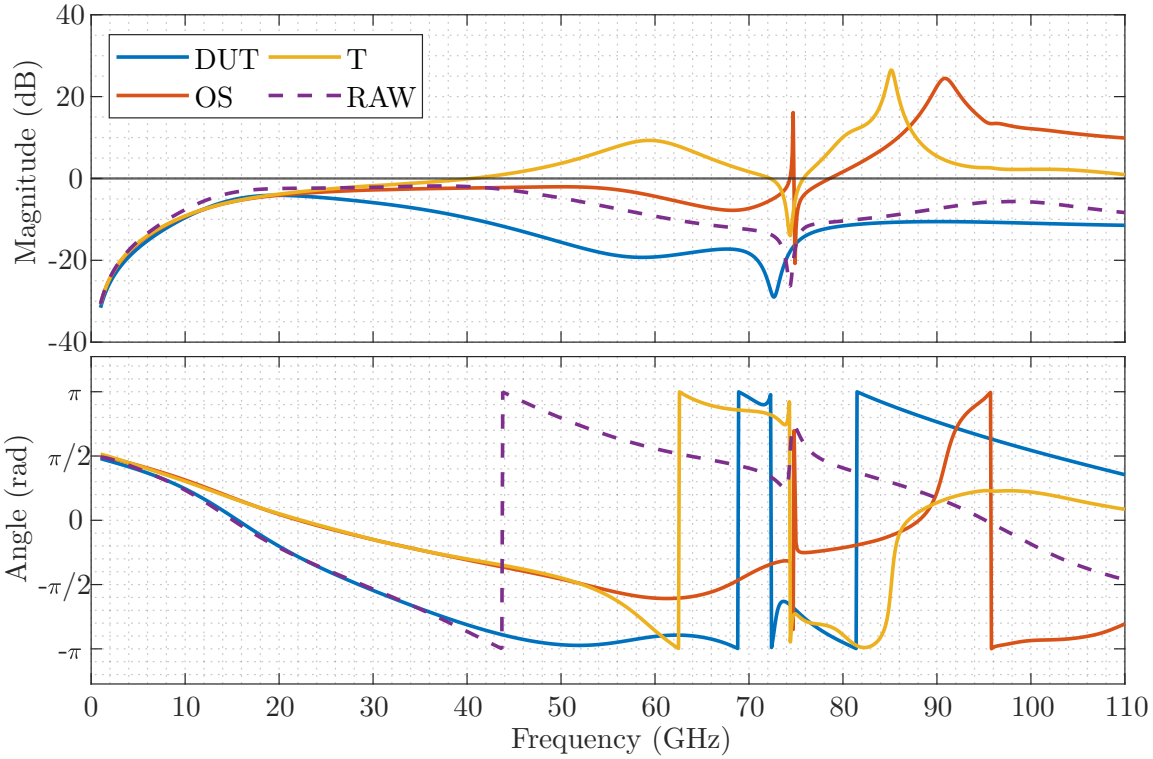

Figure 8.4. Capacitor's S_{21} parameters obtained by OPEN-SHORT and THRU de-embedding compared with RAW device and simulated DUT. The upper image is the magnitude in dB, the lower image is the phase in rad.

8.4 Inductor and Capacitor Measurement Conclusion

Throughout the process of studying de-embedding methods, numerous electromagnetic simulations were performed to determine the optimal configuration for the RAW, OPEN, SHORT, and THRU devices, aiming to obtain the best possible results. The two presented cases of inductor and capacitor simulations represent the most successful iterations achieved. However, these results suggest that these methods are not suitable for de-embedding devices fabricated on alumina substrates. The primary limitation is the dimensions of the planar devices. With thin-film technology, the smallest possible width of lines and gaps (currently, for standard use) is 50 μm, resulting in large (relative to wavelength) DUTs and extensive supporting structures. These de-embedding techniques assume that the parasitic structures behave ideally as lumped elements, a

condition generally met in integrated circuits, where these methods are mostly used [18]. However, for DUTs fabricated on alumina, these assumptions are not true and the methods fail to provide accurate measurements. Consequently, in these cases, the RAW device itself represents a more accurate measurement.

8.5 CPW Line

To support the statement in Section 8.4 that the de-embedding methods used are not suitable for devices fabricated on alumina due to dimensional limitations, a small coplanar waveguide was designed and simulated. This experiment was conducted to demonstrate that these methods can indeed be effective, but only when certain conditions are met. By reducing the dimensions of the CPW, the simulation showed that the de-embedding techniques can accurately isolate the DUT's characteristics, thus proving that the methods' ineffectiveness with larger alumina-based devices is primarily due to the size constraints. This highlights the importance of considering the physical dimensions and technological limitations when applying de-embedding methods to planar devices.

The reason for choosing the simple CPW transmission line is that its S-parameters are well-known, allowing for a clear determination of whether the de-embedding yields reasonable results. The dimensions of the DUT are presented in Table 8.1. It is important to mention that the physical geometry of the device, as used in the simulation, is not manufacturable in practical scenarios. This design choice was made solely to validate the de-embedding methods under ideal conditions, thereby demonstrating their potential effectiveness when certain dimensional constraints are met.

Table 8.1. Dimensions of the calibration standard unknown thru.

Width of middle line	Gap	Length
10 μm	7 μm	300 μm

In the Figure 8.5 is depicted the model of the RAW device the other necessary de-embedding structures, created accordingly to the Sections 6.1 and 6.2. The length of the connecting lines of the RAW device is 100 μm and length of the connection pads is 50 μm.

The structure was simulated using ACP probes, like the inductor and capacitor simulations. The first step involved correcting the measured data to shift the reference plane to the end of the probe tips. Once this was accomplished, the de-embedding methods were applied to isolate the DUT's characteristics accurately. De-embedded S-parameters of the DUT are shown in the Figures 8.6 and 8.7. At first glance, it is obvious that both scripts are functional because the data exhibit the behaviour, we would expect from a short segment of transmission line, which also confirms the blue trace of the reference DUT. This means very low reflection, high transmission and linear phase. Around 70 GHz the magnitude in dB of the transmission coefficient starts to decline and at 80 GHz differs by 0.4 dB. This deviation grows with frequency and goes up to 2 dB at 110 GHz. The phase of both S_{11} and S_{21} nearly ideally follow the reference DUT. There is also some residual error caused by the UOSM calibration, which explains why the RAW and THRU data exhibit anomalous characteristics at low frequencies. However, for the reflection coefficient, values around -80 dB (0.0001 in linear scale) far exceed the accuracy limits of the entire EM simulation.

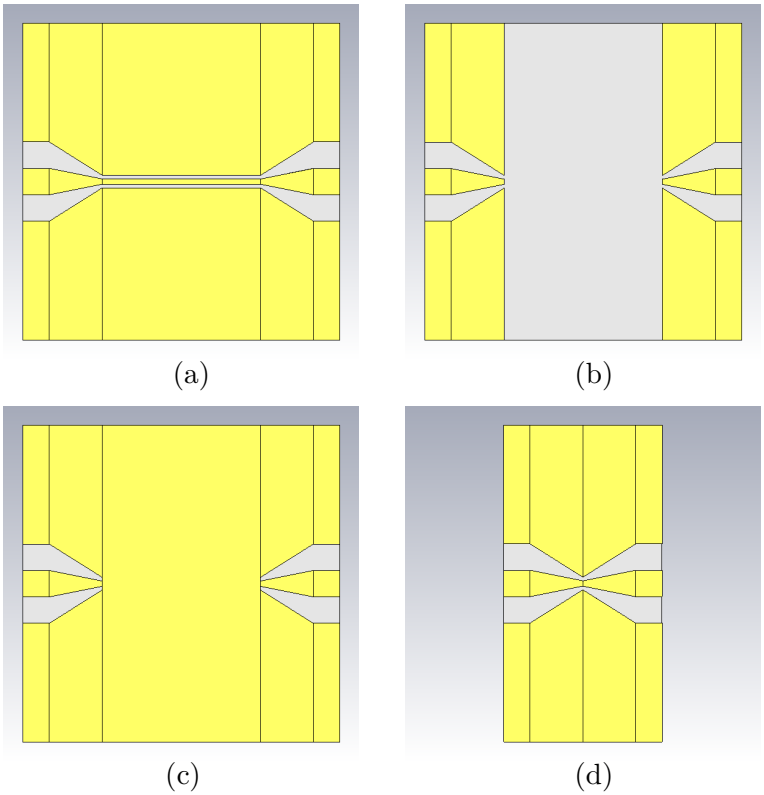

Figure 8.5. Simulated model of RAW CPW line with coplanar waveguide probes and the de-embedding structures.

Based on this evidence it can be concluded that both methods OPEN-SHORT and THRU have been correctly implemented but the dimensions of the DUT and the support structures needed the CPW probe cannot be de-embedded.

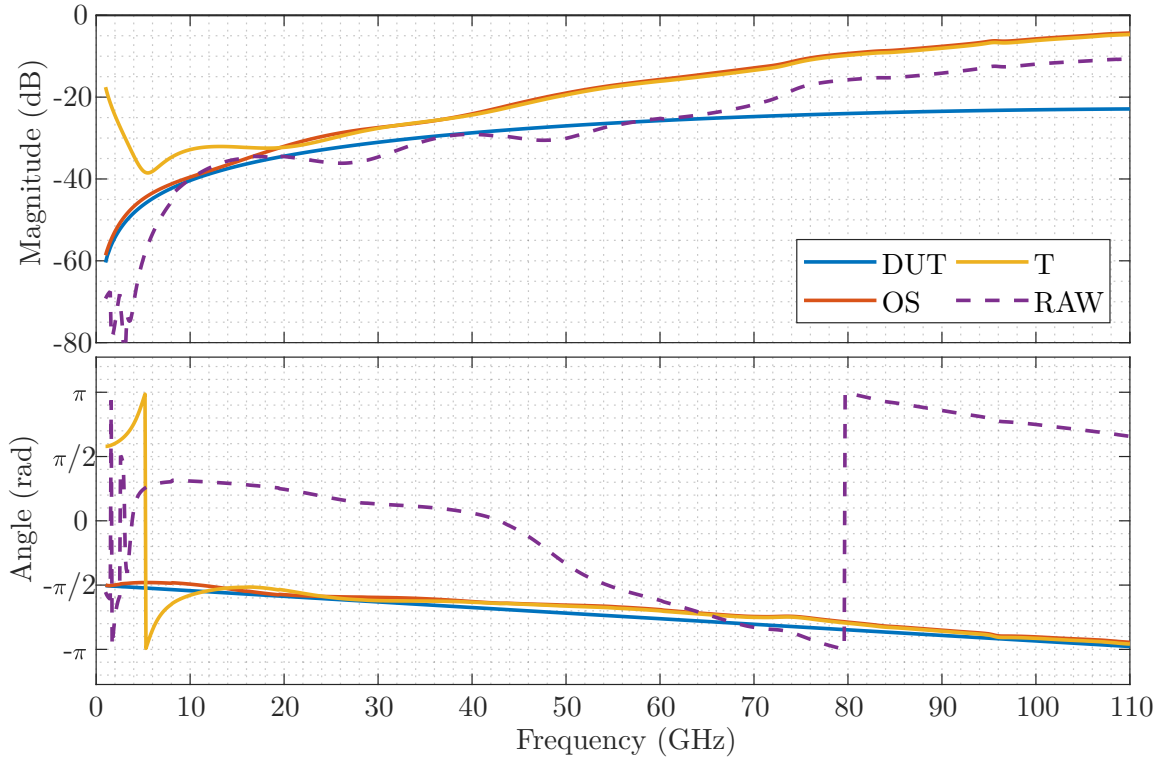

Figure 8.6. CPW line S_{11} parameters obtained by OPEN-SHORT and THRU de-embedding compared with RAW device and simulated reference DUT. The upper image is the magnitude in dB, the lower image is the phase in rad.

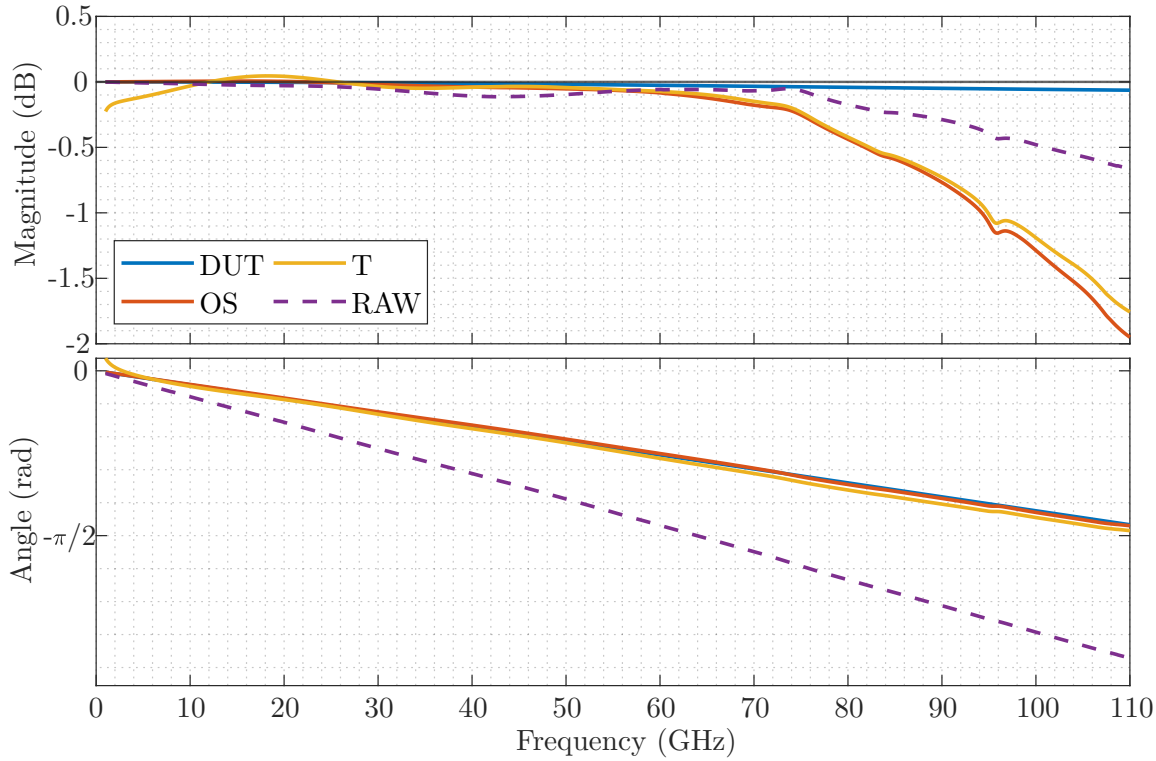

Figure 8.7. CPW line S_{21} parameters obtained by OPEN-SHORT and THRU de-embedding compared with RAW device and simulated reference DUT. The upper image is the magnitude in dB, the lower image is the phase in rad.

Chapter 9
Conclusion

The whole process of creating FormFactor coplanar air probe models (specifically ACP65-AW-GSG-250 and ACP110-AW-GSG-100) was presented in the paper. First, the development of the substrate measurement technology and the different types of probes currently in use were described. The next chapter dealt with the design of a fixture to securely mount microwave probes for the purpose of measuring their dimensions, in particular coplanar tips. Subsequently, models of both probes were created in the CST Studio Suite software and their functionality was verified by simulation. Due to the difficulty of the simulation, the models were idealised, in particular by neglecting the losses of conductors and dielectrics, which is definitely not the case in reality and the simulated S-parameters, especially the reflection coefficient S_{11}, comes out worse.

The subsequent section of this thesis addressed the implementation of the de-embedding methods OPEN-SHORT and THRU. To validate their functionality, models of an inductor, capacitor and CPW line were developed in CST Studio Suite. The DUTs were simulated using models of ACP probes, to get as close as possible to the real measurement, necessitating UOSM calibration to shift the reference plane to the probe tips. For the calibration algorithm, detailed designs and simulations of the calibration standards—open, short, match, and unknown thru—were undertaken to facilitate the calculation of error boxes. Consequently, the DUTs were de-embedded to remove the parasitic effects. The results suggest that these methods are not suitable for de-embedding devices fabricated on alumina substrates. The primary limitation is the dimensions of the planar devices. With thin-film technology, the smallest possible width of lines and gaps (currently, for standard use) is 50 μm, resulting in large (relative to wavelength) DUTs and extensive supporting structures.

For accurate evaluation of on-chip passives, the standard OPEN-SHORT de-embedding technique is not sufficient at mm-wave frequencies. Since the impedance of the OPEN de-embedding structure is lumped to a single impedance physically located at the contact pad, the impedance transformation through the lines between contact pad and DUT is not taken into account [19]. These de-embedding techniques assume that the parasitic structures behave ideally as lumped elements, a condition generally met in integrated circuits, where these methods are mostly used [18]. However, for DUTs fabricated on alumina, these assumptions are not true, and the methods fail to provide accurate measurements. Consequently, in these cases, the RAW device itself represents a more accurate measurement.

Possibility to further extend on the topic of this thesis is to implement de-embedding methods such as L-2L, which are based on distributed elements using different transmission lines to extract the parasitic characteristics [1], [19].

References

[1] Lourandakis, Errikos. *On-wafer microwave measurements and de-embedding*. Artech House, 2016.

[2] Rumiantsev, Andrej, and Ralf Doerner. RF Probe Technology: History and Selected Topics. *Microwave Magazine, IEEE*. 11, 2013, Vol. 14, pp. 46-58. Available from DOI 10.1109/MMM.2013.2280241.

[3] FormFactor, Inc. *Probe Selection Guide*. Available from `https://www.formfactor.com/download/probe-selection-guide/?wpdmdl=2561&refresh=65ca236901dc61707746153`.

[4] Strid, E.. *On-Warer Measurements with the HP 8510 Network Analyzer and Cacade Microtech Wafer Probes* [RF & Microwave Measurement Symposium and Exhibition].

[5] Boll, Gregory G. BollHarry J.. *Integrated circuit probing apparatus*. Available from `https://patents.google.com/patent/US4871964A/en`.

[6] Godshalk, Edward M., Jeremy Burr, and Jeff Williams. An Air Coplanar Wafer Probe. In: *1994 24th European Microwave Conference*. 1994. pp. 1380-1385. Available from DOI 10.1109/EUMA.1994.337408.

[7] Aguilera, Jaime, and Roc Berenguer. *Design and Test of Integrated Inductors for RF Applications*. Kluwer Academic Publishers, 2004. ISBN 978-1441954114.

[8] Rumiantsev, Andrej, Ralf Doerner, and Edward M. Godshalk. The influence of calibration substrate boundary conditions on CPW characteristics and calibration accuracy at mm-wave frequencies. In: *2008 72nd ARFTG Microwave Measurement Symposium*. 2008. pp. 168-173. Available from DOI 10.1109/ARFTG.2008.4804293.

[9] Safwat, Amr M. E., and Leonard Hayden. Sensitivity Analysis of Calibration Standards for SOLT and LRRM. In: *58th ARFTG Conference Digest*. 2001. pp. 1-10. Available from DOI 10.1109/ARFTG.2001.327488.

[10] Collier, R.J., A.D. Skinner, Institution of Engineering, and Technology. *Microwave Measurements*. Institution of Engineering and Technology, 2007. IET electrical measurement series Microwave measurements. ISBN 9780863417351. Available from `https://books.google.cz/books?id=jhzfMLh9gFoC`.

[11] Bauer, R.F., and P. Penfield. De-Embedding and Unterminating. *IEEE Transactions on Microwave Theory and Techniques*. 1974, Vol. 22, No. 3, pp. 282-288. Available from DOI 10.1109/TMTT.1974.1128212.

[12] Issaoun, Ammar, Yong Zhong Xiong, Jinglin Shi, James Brinkhoff, and Fujiang Lin. On the Deembedding Issue of CMOS Multigigahertz Measurements. *IEEE Transactions on Microwave Theory and Techniques*. 2007, Vol. 55, No. 9, pp. 1813-1823. Available from DOI 10.1109/TMTT.2007.904041.

[13] Koolen, M.C.A.M., J.A.M. Geelen, and M.P.J.G. Versleijen. An improved de-embedding technique for on-wafer high-frequency characterization. In: *Proceedings*

of the 1991 Bipolar Circuits and Technology Meeting. 1991. pp. 188-191. Available from DOI 10.1109/BIPOL.1991.160985.

[14] Tiemeijer, L.F., and R.J. Havens. A calibrated lumped-element de-embedding technique for on-wafer RF characterization of high-quality inductors and high-speed transistors. *IEEE Transactions on Electron Devices*. 2003, Vol. 50, No. 3, pp. 822-829. Available from DOI 10.1109/TED.2003.811396.

[15] Microelectronics, Cicor. *PCBs & Hybrids Design Manual*. Available at `https://www.cicor.com/en/downloads/design-manuals/`.

[16] Sia, Choon Beng, Beng Hwee Ong, Kwok Wai Chan, Kiat Seng Yeo, Jian-Guo Ma, and Manh Anh Do. Physical layout design optimization of integrated spiral inductors for silicon-based RFIC applications. *IEEE Transactions on Electron Devices*. 2005, Vol. 52, No. 12, pp. 2559-2567. Available from DOI 10.1109/TED.2005.859638.

[17] Shafi, K. T. Muhammed, Varuna Baipadi, and Venkata Vanukuru. Layout Optimization of Short De-embedding Structure for Accurate On-Chip Inductor Characterization. In: *2021 IEEE 20th Topical Meeting on Silicon Monolithic Integrated Circuits in RF Systems (SiRF)*. 2021. pp. 31-33. Available from DOI 10.1109/SiRF51851.2021.9383413.

[18] Yau, Kenneth H. K., Ioannis Sarkas, Alexander Tomkins, Pascal Chevalier, and Sorin P. Voinigescu. On-wafer S-parameter de-embedding of silicon active and passive devices up to 170 GHz. In: *2010 IEEE MTT-S International Microwave Symposium*. 2010. pp. 600-603. Available from DOI 10.1109/MWSYM.2010.5518218.

[19] Veenstra, H., M. G. M. Notten, D. van Goor, and J. B. Mills. Distributed de-embedding technique for accurate on-chip passive measurements based on Open-Short structures. In: *2009 IEEE Bipolar/BiCMOS Circuits and Technology Meeting*. 2009. pp. 91-94. Available from DOI 10.1109/BIPOL.2009.5314136.

Appendix A
MATLAB Script OPEN-SHORT De-Embedding

```
function [s_dut] = OpenShortDeembedding(s_raw, s_open, s_short)
%%  OpenShortDeembedding uses measured S-parameters of OPEN and SHORT
%       models to get direct S-prameters of DUT itself
%    - implemented for 2-port devices
%    - removes influence of contact pads and lead transmission lines
%    - s_raw, s_open, s_short:
%        - dimensions: [2 x 2 x nFreq]
%        - Complex double
%
%    Implemented acording to:
%               Lourandakis, Errikos. On-wafer microwave measurements
%                   and de-embedding. Artech House, 2016.
%
% @ 2024, Jan Šmolcnop

    %% Convert S-parameters to Y-parameters
    %    - using functions from RF Toolbox
    y_raw = s2y(s_raw, 50);
    y_open = s2y(s_open, 50);
    y_short = s2y(s_short, 50);

    % Remove OPEN shunt admittance Y from RAW
    y_ro = y_raw - y_open;
    % Convert to Z-parameters
    z_ro = y2z(y_ro);

    % Remove OPEN shunt admittance from SHORT
    y_so = y_short - y_open;
    % Convert to Z-parameters
    z_so = y2z(y_so);

    % Remove remaining series impedance
    z_dut = z_ro - z_so;

    % Convert to S-parameters to obtain de-embedded parameters
    s_dut = z2s(z_dut, 50);
end
```

Appendix B
MATLAB Script THRU De-Embedding

```
function [s_dut] = ThruDeembedding(s_raw, s_thru)
%%  ThruDeembedding uses measured S-parameters of THRU model
%       to get direct S-prameters of DUT itself
%    - implemented for 2-port devices
%    - removes influence of contact pads and lead transmission lines
%    - s_raw, s_thru:
%        - dimensions: [2 x 2 x nFreq]
%        - Complex double
%
%    Implemented acording to:
%               Lourandakis, Errikos. On-wafer microwave measurements
%                   and de-embedding. Artech House, 2016.
%
% @ 2024, Jan Šmolcnop

    %% Convert RAW S-parameters to T-parameters
    t_raw = s2t(s_raw);

    % Get Y11 and Y12 parameters of THRU
    y_thru = s2y(s_thru);
    y11_thru = y_thru(1,1,:);
    y12_thru = y_thru(1,2,:);

    % Define Left and Right matrices of THRU
    y_left = [y11_thru-y12_thru, 2*y12_thru;...
                2*y12_thru, -2*y12_thru];

    y_right = [-2*y12_thru, 2*y12_thru;...
                2*y12_thru, y11_thru-y12_thru];

    % Convert Y-parameters to T-parameters
    s_left = y2s(y_left);
    s_right = y2s(y_right);

    t_left = s2t(s_left);
    t_right = s2t(s_right);

    % Compute DUT T-parameters
    tmp = pagemldivide(t_left, t_raw);
    t_dut = pagemrdivide(tmp, t_right);
```

```
    % Convert T-parameters to S-parameters of DUT
    s_dut = t2s(t_dut);

end
```